



**Final Zoning of Earth Fissure Risk & Determination
Of Part(s) of the Dam that Require
Dam Safety Modifications
McMicken Dam Fissure Risk Zone Remediation Project
Contract FCD 2002C011, Work Assignment No. 2A**

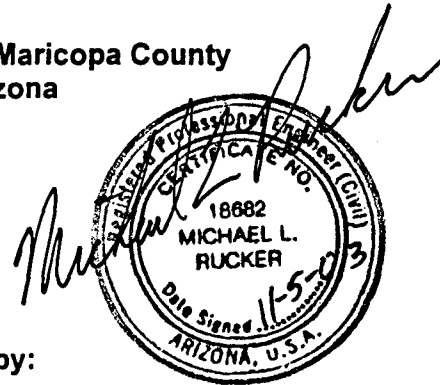


Property of
Flood Control District of MC Library
Please Return to
2801 W. Durango
Phoenix, AZ 85009

**Final Zoning of Earth Fissure Risk & Determination
Of Part(s) of the Dam that Require
Dam Safety Modifications
McMicken Dam Fissure Risk Zone Remediation Project
Contract FCD 2002C011, Work Assignment No. 2A**

Submitted to:

**Flood Control District of Maricopa County
Phoenix, Arizona**



Submitted by:

**AMEC Earth & Environmental, Inc.
Phoenix, Arizona**

5 November 2003

AMEC Job No. 2-117-001066



5 November 2003
AMEC Job No. 2-117-001066

Bobbie Ohler, P.E.
Flood Control District of Maricopa County
2801 West Durango Street
Phoenix, Arizona 85009-6399

Dear Ms. Ohler:

**Re: Final Zoning of Earth Fissure Risk & Determination
of Part(s) of the Dam that Require Dam Safety Modifications
McMicken Dam Fissure Risk Zone Remediation Project
Contract FCD 2002C011, Work Assignment No. 2A**

Transmitted herewith are eight copies of the memorandum presenting the computer modeling completed for McMicken Dam to further define the fissure risk zone. The memorandum discusses the model used, the sections analyzed and the parameters assumed. It also presents a summary of models used by others to simulate land subsidence, horizontal movements and horizontal strains resultant of groundwater withdrawal.

Should you have any questions, please do not hesitate in contacting the undersigned.

Respectfully submitted,

AMEC Earth & Environmental



Michael R. Rucker, P.E.
Senior Engineer

Reviewed by:



Lawrence A. Hansen, P.H.D., P.E.
Senior Vice President

G:\Engineering Department\2002 Projects\2-117-001066 McMicken Dam Fissure Risk Zone\Task 2A-Final Zoning-Earth FissureModRptRevUntrk.doc

c: Addressee (8)

AMEC Earth & Environmental, Inc.
3232 West Virginia Avenue
Phoenix, Arizona 85009-1502
Tel: (602) 272-6848
Fax: (602) 272-7239

www.amec.com



TABLE OF CONTENTS

		Page
1.0	INTRODUCTION	1
2.0	EARTH FISSURE MODELING AND MEASUREMENT.....	1
3.0	INITIAL ANALYSES.....	4
4.0	ANALYSIS OF GROUND SUBSIDENCE AND DEFORMATION	5
4.1	Analysis Procedures.....	5
4.2	Model Input Parameters	6
	4.2.1 Bedrock	6
	4.2.2 Basin Alluvium	6
	4.2.3 Changing Water Levels.....	8
	4.2.4 Survey and InSAR Subsidence Data	9
5.0	SECTION A-A'	10
5.1	Section A-A' Profile.....	10
5.2	Section A-A' Calibration.....	11
5.3	Modeled Subsidence and Subsidence Predictions	12
5.4	Modeled Horizontal Strain and Horizontal Strain Predictions	12
6.0	SECTION B-B'	13
6.1	Section B-B' Profile.....	13
6.2	Section B-B' Calibration.....	14
6.3	Modeled Subsidence and Subsidence Predictions	15
6.4	Modeled Horizontal Strain and Horizontal Strain Predictions	15
7.0	SECTION C-C'	16
7.1	Section C-C' Profile	16
7.2	Section C-C' Calibration	16
7.3	Modeled Subsidence and Subsidence Predictions	17
7.4	Modeled Horizontal Strain and Horizontal Strain Predictions	17
8.0	SECTION D-D'	18
8.1	Section D-D' Profile	18
8.2	Section D-D' Calibration	18
8.3	Modeled Subsidence and Subsidence Predictions	19
8.4	Modeled Horizontal Strain and Horizontal Strain Predictions	19
9.0	DISCUSSION AND CONCLUSIONS	19
	REFERENCES	22

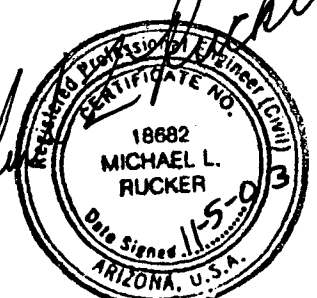
TABLE OF CONTENTS

Page

LIST OF FIGURES

Figure 1	Site Plan with Conceptual Interpreted Clay Elevation
Figure 2	Lee and Shen Analysis – McMicken Dam Section B-B' Case X-1
Figure 3	Lee and Shen Analysis – McMicken Dam Section B-B' Case X-2
Figure 4	Lee and Shen Analysis – McMicken Dam Section B-B' Case Y-1
Figure 5	Lee and Shen Analysis – McMicken Dam Section B-B' Case Y-2
Figure 6	Well Histories & Modeled Water Levels over Time
Figure 7	Profile Section A-A'
Figure 8	Section A-A' Calibration (1947-1981; NGS) (modulus variable over time)
Figure 9	Section A-A' (variable modulus) Modeled Subsidence
Figure 10	Section A-A' (variable modulus) Modeled vs. InSAR Subsidence
Figure 11	Section A-A' (variable modulus) Modeled Horizontal Strain
Figure 12	Section A-A' Calibration (1947-1981; NGS) (modulus constant over time)
Figure 13	Section A-A' (modulus constant) Modeled Subsidence
Figure 14	Section A-A' (modulus constant) Modeled vs. InSAR Subsidence
Figure 15	Section A-A' (modulus constant) Modeled Horizontal Strain
Figure 16	Profile Section B-B' – Original Geometry (Geometry-1)
Figure 17	Section B-B' Initial Calibration Attempt (before gravity re-interpretation)
Figure 18	Profile Section B-B' Revised Geometry (Geometry-4)
Figure 19	Section B-B' Calibration (1955-1982; SHB, 1982) after Gravity Re-interpretation of Bedrock Contact
Figure 20	Section B-B' Modeled vs. Observed Subsidence
Figure 21	Section B-B' Modeled Subsidence
Figure 22	Section B-B' Modeled Horizontal Strain
Figure 23	Profile Section C-C'
Figure 24	Section C-C' & D-D' Subsidence Calibration (1947-1981; NGS)
Figure 25	Section C-C' InSAR vs. Modeled Subsidence
Figure 26	Section C-C' Modeled Subsidence
Figure 27	Section C-C' Modeled Horizontal Strain
Figure 28	Profile Section D-D'
Figure 29	Section D-D' (1992-1999) Modeled vs. InSAR Subsidence
Figure 30	Section D-D' Modeled Subsidence
Figure 31	Section D-D' Modeled Horizontal Strain

Michael L. Rucker





Flood Control District of Maricopa County
Final Zoning of Earth Fissure Risk & Determination
of Part(s) of the Dam that Require Dam Safety Modifications
McMicken Dam Fissure Risk Zone Remediation Project
Contract FCD 2002C011, Work Assignment No. 2A
AMEC Job No. 2-117-001066
5 November 2003

1.0 INTRODUCTION

This memorandum prepared by AMEC Earth & Environmental, Inc. (AMEC) presents the results of numerical analyses of land subsidence, horizontal deformation and horizontal strain induced by groundwater withdrawal for sections along and adjacent to the south end of McMicken Dam. The general purpose of the modeling effort was to further delineate to the extent practical the fissure risk zones previously determined by AMEC (2003)¹. In particular, the intent is to model a section along the dam extending through the high and moderate fissure hazard zones to determine if horizontal strains have developed that may result in earth fissure features, thus requiring modification of the fissure risk zones. The intent also is to use the model to estimate future horizontal strains in order to determine if sufficient strain could develop that would result in earth fissuring, and what groundwater declines would be required to create the horizontal strain.

This memorandum was prepared as part of the alternative analysis being completed for the Flood Control District of Maricopa County, herein referred to as the District. The modeling and the related tasks described herein was conducted for the District in accordance with the McMicken Dam Fissure Risk Zone Remediation (FRZR) Project, Work Assignment 2A of Contract FCD 2002C011 between AMEC and the District. The purpose of the McMicken Dam FRZR Project is to mitigate the risk associated with the earth fissures that have been identified near the south end of the dam, and which may intersect the dam and its foundation. The intent of the alternatives analysis process is to select a preferred alternative for mitigation of the fissure risk zone, thereby enhancing the safety of dam. The final report for the project will present a preliminary design (15 percent plans) for the preferred alternative.

2.0 EARTH FISSURE MODELING AND MEASUREMENT

Three elastic models that have been used to explain earth fissure development and movement are (1) bending of a plate or beam above a horizontal discontinuity in compressibility (Lee and Shen, 1969), (2) dislocation theory representing a fault or tensile crack (Holzer and others, 1979; Carpenter 1993) and (3) compressibility (Haneberg, 1992). These three mechanisms probably act together at all earth fissures and are grouped in the term "generalized differential compaction". In each case, the horizontal discontinuity can be an edge of a bedrock bench, a mountain-bounding fault, a high in the underlying bedrock or a facies change. The driving force is differential compaction caused by increased effective stress, which is in turn caused by aquifer-system hydraulic head decline.

¹ References are listed at the end of this report.

Land subsidence and associated earth fissure development due to dewatering has been recorded in the past (USGS Circular 1182) in the following areas: Santa Clara Valley, California; San Joaquin Valley, California; Las Vegas, Nevada; south central Arizona; and Houston and Galveston, Texas. A study was conducted near Picacho in south-central Arizona from 1980 to 1984 (Carpenter, 1993) to monitor vertical and horizontal displacement along a single survey line normal to the Picacho earth fissure. The survey line consisted of nine closely spaced monuments for tape extensometer measurements and leveling located near the fissure, and eight widely spaced monuments for electronic distance measurements and leveling elsewhere along the line. From May 1980 to May 1984, the western, downthrown side of the fissure subsided 167 mm (6.57 inches) and moved 18 mm (0.71 inch) westward into the basin. Concurrently, the eastern, relatively upthrown side subsided 147 mm (5.79 inches) and moved 14 mm (0.55 inch) westward.

Jachens and Holzer (1982) computed horizontal tensile strain associated with eight earth fissures in these areas. Both analytical and numerical (finite element) methods were used to estimate the horizontal displacement and strain. The calculated strains at failure are tensile and ranged from approximately 0.02 percent to 0.2 percent, with most falling in the range 0.02 percent to 0.06 percent. These data suggest that the threshold for earth fissure initiation is 0.02 percent horizontal stain, though earth fissures do not always develop at this low value of strain. For the purposes of this report, a value of 0.02 percent strain is adopted as the threshold value for earth fissure development.

The effect of ground water pumping on earth fissures in south central Arizona was investigated through field measurements by researchers at the University of Arizona (Boling, et al., 1980). Bimonthly horizontal movement measurements of earth fissures using seven dial gauge extensometers were made over a three-year period near Signal Peak, the Pichacho Mountains, and in Avra Valley. Earth fissures closed during long dry periods and opened after high rainfall events. After a period of high pumping followed by high rainfall, it was noted that earth fissures typically opened. The largest total measured movement (sum of opening and closing measurements of all fissures) across the group of earth fissures was 20.27 mm (0.8 inch), and the largest single movement (opening or closing measurement for only a single fissure) was 30 mm (1.18 inch). In one single event, a rainfall of 31 mm (1.22 inch) resulted in one earth fissure opening approximately 25 mm (1 inch), with a nearby earth fissure opening 1.6 mm (0.06 inch) and another parallel earth fissure closing 2.1 mm (0.08 inch).

Land subsidence and earth-fissure hazards near Luke Air Force Base have been reported by the USGS (Schumann, 1994). Ground-water declines of more than 300 feet have caused the aquifer materials to compact and by 1991 had resulted in as much as 18 feet of land subsidence. Earth fissure zones as long as 2 miles occur on the periphery of the areas of maximum land subsidence on three sides of the base. When an earth fissure captures surface

flows, the fissure enlarges by rapid erosion of the sides, by slumping and piping along the trend of fissures. Such erosion produced open fissure gullies as deep as 15 feet deep and as wide as 30 to 40 feet in local areas.

Subsidence in the Las Vegas valley has been monitored by the USGS (Bell, et al., 2002) since 1935 and subsidence of more than 5 feet has been reported. A compilation of subsidence rates based on conventional leveling, InSAR and GPS data for 1978 through 1999 indicates that rates have significantly declined since 1991 because of an artificial recharge program. The artificial recharge program has produced a general rise in the water table, arresting subsidence in most parts of the valley except for the northwest bowl, where movement still continues at a stable rate 2.5 to 3 cm (1 to 1.2 inches) per year, though a rate of 5 to 6 cm (2 to 2.4 inches) per year was observed from 1978 to 1991.

The USGS developed three Inter-Bed-Storage package models (IBS 1, 2 and 3) (Leake, 1992) to be used with MODFLOW, a widely used finite difference groundwater flow model. IBS1 presently is the only commercially available model. The IBS1 package assumes that elastic deformation of the aquifer system is proportional to changes in the effective stress. IBS1 inherently assumes that changes in hydraulic head in aquitards equilibrate with changes in aquifers within a single time step, thus delayed drainage could not be modeled. The IBS packages can only estimate vertical subsidence; the associated horizontal movement is not modeled.

Leake and Hsieh (1995) compared the MODFLOW model also known as the Terzaghi model with another two-dimensional finite element solution of flow and deformation. In the second model, which is known as Biot's model, the matrix deformation due to effective stress is described by Biot's constitutive relationships and by stress equilibrium. Comparing the two methods, it is shown that the simpler Terzaghi method adequately describes deformation on a regional scale. For analysis of smaller-scale deformation around a localized feature such as a bedrock step, the more rigorous Biot method can be used to calculate potential horizontal strains that lead to development of earth fissures.

Historical land subsidence observations at benchmarks and recent InSAR-derived subsidence data were used to model the compaction time constants and inelastic deformation of compacting inter-bed layers in a coupled regional groundwater flow and aquifer system compaction model of Antelope Valley, California (Hoffmann, et al., 2003). The numerical model used a modified MODFLOW program along with the non-linear parameter estimation program UCODE to improve calibration between simulated and observed land subsidence, both in terms of magnitude and spatial extent. However, the ability of the model to adequately reproduce the subsidence observed over only a few years (short-term interval) was impaired by the fact that the simulated hydraulic heads are often not representative of the actual aquifer hydraulic heads.

InSAR derived ground displacement data proved extremely valuable in mapping recent subsidence and in developing numerical subsidence models. The InSAR data was extensively used in subsidence modeling, particularly in defining parameter zones for the modeling for Antelope Valley, California (Hoffmann, et al., 2003) and the Las Vegas valley in Nevada (Hoffmann, et al., 2001). Those techniques also were applied to detect the deformed area due to land subsidence in Jakarta, Indonesia (Hirose, et al., 2001). InSAR derived data matched well with the extensometer measurements where most of the subsidence was confined to shallow depths. Deep compaction occurring below the anchored depth of an extensometer can cause significant differences in the subsidence observed by InSAR and the compaction measured by extensometers (Hoffmann, et al., 2001).

3.0 INITIAL ANALYSES

Lee and Shen (1969) provided a simplified method for the evaluation of horizontal movements and strains due to subsidence. In the analysis, it is assumed that soil above the groundwater table acts as a rigid beam over compressible sediments. As applied to subsidence at the McMicken Dam site, the thickness of the upper stiff layer, which does not participate directly in the subsidence, but simply moves downward as lower layers compress, is very important to the analysis. In the Lee and Shen analysis the upper stiff layer behaves like a thick plate, which bends to conform to the vertical movements necessary to maintain continuity with the lower layers as they compress. The horizontal movement, m , of a point A on the surface is defined by

$$m = 2/3 H \alpha$$

where

H = the thickness of the upper stiff layer, and
 α = the slope of the subsidence profile at Point A.

In general, if the vertical subsidence along a profile is known, the horizontal movement and strain can be readily estimated using above equation.

The horizontal displacement and strain were estimated for a part of Section B-B' (Stations 40+00 to 120+00) for McMicken Dam (see Figure 1) using the Lee and Shen (1969) method. Initially, for simplicity the analyses assumed a constant thickness of the upper stiff layer (H), however, four final cases were analyzed assuming a variable thickness. For the analyses, the thickness H was assumed constant between Stations 40+00 and about 65+00. For Case X-1 shown in Figure 2, the constant value of H was 25 feet, increasing to 250 feet at Station 120+00. For Case X-2 shown in Figure 3, the constant value of H was 50 feet, increasing to 250 feet at Station 120+00. For Cases Y-1 and Y-2 (Figures 4 and 5, respectively), the values of H were assumed to twice those assumed for Cases X-1 and X-2, in order to evaluate the sensitivity of the procedure to this parameter. For all analyses, the vertical subsidence was

assumed to be zero feet from Stations 40+00 to 60+00, then increasing almost linearly to 4.5 feet at Station 117+50. This subsidence approximates the subsidence between 1955 and 1982, based on a comparison of a survey completed in 1982 with the presumed as-built crest elevation of McMicken Dam (Figure 17, SHB, 1982).

As indicated by the horizontal strain profiles in Figures 2 through 5, the maximum values of horizontal (negative) strain occur at about Stations 100+00 and 117+50. For Cases X-1 and X-2, which assumed a lesser stiff upper layer thickness, the maximum horizontal strain is about 0.013 percent. This is less than the approximate lower bound 0.02 percent strain threshold for earth fissure initiation discussed in the previous section of this report. When the upper layer thickness is increased by a factor of two, as shown for Cases Y-1 and Y-2, the maximum horizontal strain increases to about 0.026. This is a direct result of the above equation, where the horizontal movement, and hence the horizontal strain, is indicated to be directly proportional to the value of the upper layer thickness, H. The maximum value of the computed strain for these cases exceeds the threshold value. The Lee and Shen analyses did indicate the potential for the known subsidence to result in earth fissure initiation, but they also indicated that to better evaluate the causes of the existing fissures and the potential for future fissure development methods incorporating more completely the geology underlying the site were required.

4.0 ANALYSIS OF GROUND SUBSIDENCE AND DEFORMATION

4.1 Analysis Procedures

Analysis of ground subsidence and deformation was performed using 2-D numerical models for four cross-sections along or through portions of McMicken Dam and adjacent areas (see Figure 1). Modeling subsidence and deformation of the alluvium in response to changes in groundwater levels in the aquifer system required addressing displacements and pore water pressure changes simultaneously. This coupling was achieved with use of two finite element based computer programs, SEEP/W and SIGMA/W, developed by Geoslope (1998). SIGMA/W computes displacements and stresses, and SEEP/W computes the changes in pore-water pressure with time. Using these two software products in a coupled manner made it possible to perform reasonable subsidence and deformation analyses for specified time periods.

When coupled, both SIGMA/W and SEEP/W contribute to forming a common global characteristic (stiffness) matrix. Three equations are created for each node in the finite element mesh. Two are equilibrium (displacement) equations formed by SIGMA/W and the third is a continuity (flow) equation formed by SEEP/W. Solving all three equations simultaneously determines both displacement and pore-water pressure changes. In SIGMA/W, force and displacement boundary conditions are assumed, and soil properties are defined using effective stress parameters. In SEEP/W, head and flow boundary conditions are assumed, with hydraulic conductivity and volumetric water content functions specified.

4.2 Model Input Parameters

The computer modeling required three materials to define the two-dimensional geometry, including bedrock, higher modulus (stiffer) higher permeability alluvium, and lower modulus (softer) lower permeability alluvium. In addition, changes in water levels also were required. Elastic modulus (representative of stress-strain response) and hydraulic conductivity values were assigned to the bedrock and alluvial units based on the descriptions provided for them in AMEC (2003). These parameters, including the location of the bedrock and alluvial units and their properties, were varied to compute various ground subsidence profiles, which were then compared to measured subsidence from surveys or from interferograms. Variations in the profiles and manipulation of the basic parameters to match measured subsidence over modeled time served to calibrate the model profiles. Once calibrated, the models were extended forward through time to predict estimated future subsidence and horizontal strains.

4.2.1 Bedrock

The depths to bedrock in the modeled profiles were initially based on interpretations of gravity surveys with calibration by ReMi seismic profiles as presented in AMEC (2003). During the calibration of the model for Section B-B' (see Figure 1) along the dam centerline, it was determined that the initial gravity interpretation for that section was not reasonable. The presence of a relatively thin lower density clayey lens, beginning at about Station 93+00 and extending beyond the model profile at about Station 140+00, was not accounted for in the initial gravity interpretation presented in AMEC (2003). The gravity profile along this section was re-interpreted to include the relatively thin clayey lens.

The depth to bedrock also was re-interpreted to be deeper than initially considered, and the resulting modeled subsidence was an improved match to the actual measured subsidence. Bedrock profiles for Sections B-B', C-C' and D-D' also were modified to reflect this revised interpretation. Parameters assumed for the bedrock included an elastic modulus value of 9.71×10^6 pounds per square foot (psf) and a hydraulic conductivity of 1×10^{-4} feet per day (ft/d).

4.2.2 Basin Alluvium

Two types of basin alluvium were included in the models, an Upper Alluvium Unit (UAU) and a more clayey Fine-grained Unit (FGU). The distribution of the FGU was interpreted through interferograms, of which Figure 1 is an example, and the results of deep resistivity soundings presented in AMEC (2003). The deeper basin alluvium known as the Middle Fine-grained Unit (MFGU) is ignored in the modeling, and is considered to be a boundary condition similar to bedrock.

Upper Alluvium Unit (UAU)

UAU alluvium modulus and hydraulic conductivity values were selected to provide a relatively rapid component to the modeled subsidence. Geophysical measurements presented in AMEC (2003) assisted in selecting relevant alluvium parameters. Measured resistivity values that exceed 1,000 ohm-cm, and more typically are in the range of 2,000 to 6,000 ohm-cm, indicate that some clay fraction is present in the UAU, but that significant clay behavior probably would not control this material. Similarly, ReMi shear wave velocities typically in the range of 3,000 to 4,700 ft/sec indicate that the UAU materials have moderate elastic modulus values. UAU model parameters included elastic modulus values in the range of 1×10^6 to 2×10^6 psf and hydraulic conductivity values in the range of 1 to 3 ft/d.

Significant portions of the InSAR imagery for the region indicates that relatively little differential subsidence was occurring in the mid to late 1990's, such as the green areas in Figure 1. Relatively high permeability values for the UAU result in subsidence that occurs rapidly with changing water levels. The green areas in Figure 1 had undergone significant subsidence prior to 1981, as indicated by survey on the NGS line at the Beardsley Canal (AMEC, 2003). However, with stable groundwater levels through the 1990's, the subsidence was substantially complete and relatively little differential subsidence was occurring since the early to mid-1990s. Calibration of modeled versus measured subsidence occurring prior to 1981 along the various profiles was accomplished primarily through manipulation of the UAU alluvium parameters.

Clayey Alluvium Fine-Grained Unit (FGU)

InSAR data and geophysical concurrence (AMEC, 2003) indicate the presence of a significant zone of more clayey alluvium (FGU), as shown by the subsidence bowl in Figure 1. The color changes in Figure 1 depict changes in elevation for the 36-month long time frame indicated. The blue area is the approximate center of the subsidence bowl. Resistivity values in the range of 500 to 700 ohm-cm that were interpreted for deep soil horizons indicate the presence of materials with significant clay content. Modeling a clayey FGU in the profiles required a means to estimate a relative thickness for the clayey FGU. The high point of this zone on Section A-A' was estimated from deep resistivity readings. The hydrograph for Well 612994, as shown in Figure 6, provided evidence of a minimum bottom for the horizon. Well 612994, which was drilled to a relatively shallow depth of 534 feet, has exhibited a behavior trend different from other wells in the area. After water levels dropped at a rate similar to other wells prior to the mid-1960s, the water levels abruptly rose and have maintained a higher elevation than observed in other wells since. An interpretation of that behavior is that Well 612994 extends into the clayey FGU but does not penetrate through the FGU.

It appears likely that pumping of the well dropped the water level into the FGU, where well performance degraded. Pumping of the well was stopped in the mid-1960s. The water level then recovered until reaching the top of the FGU. Thus, Well 612994 provides a possible top of the FGU at the well's location, and provides a minimum bottom to the FGU. The conceptual thickness of the clayey FGU was then estimated from its top elevation as derived from resistivity data, and its bottom elevation as derived from the well data. InSAR imagery contours were then used to represent and distribute the change in FGU thickness for model Sections A-A', B-B', C-C' and D-D'.

Significant portions of the InSAR imagery for the region indicates the locations where differential subsidence was occurring in the mid to late 1990s, such as the subsidence bowl crossed by Section A-A' in Figure 1. Relatively low permeability values for the FGU result in subsidence that occurs slowly with changing water levels. Subsidence prior to 1981, as indicated by survey of the NGS line at the Beardsley Canal and the survey of the McMicken Dam crest elevation (SHB, 1982), was significantly greater than the recent subsidence indicated by InSAR data and current survey data (FCDMC, 2001). However, with stable groundwater levels through the 1990s, the slow subsidence in the FGU has been a relatively more significant portion of the subsidence occurring more recently, particularly since the early to mid-1990s. Calibration of modeled versus measured subsidence occurring between 1992 and 1999 or the present along the various profiles was accomplished primarily through manipulation of the FGU parameters. Assumed FGU parameters included elastic modulus values in the range of 2.0×10^5 to 2.5×10^5 psf and a hydraulic conductivity value of 0.01 f/d.

An interesting characteristic of the FGU derives from its slow draining and, thus, time delayed subsidence behavior. Under conditions of rapid water level drop, relatively little consolidation and subsidence occurs in the FGU, while substantial subsidence occurs in the UAU. During this time the short-term effects of the relatively rigid FGU on stress and strain concentrations in the alluvial basin are similar to the effects of rigid bedrock.

4.2.3 Changing Water Levels

Water level well hydrographs for the area, as reported in AMEC (2003), are presented in Figure 6. It should be noted that the closest sources for water level data along McMicken Dam are the wells located along the Beardsley Canal. A single water level reading taken at a well west of the dam in the early 1980s is assumed representative of water levels in the alluvium west of the dam, and is similar to water levels in the alluvium east of the dam.

General water level trends used in the models are also presented in Figure 6. Model profile Sections A-A', C-C' and D-D' are oriented roughly perpendicular to McMicken Dam, while Section B-B' is oriented along the dam. It is assumed that groundwater flow through the alluvial basin has been at least roughly perpendicular to the axis of the dam. Flow through profile

Sections A-A', C-C' and D-D' was reasonably modeled by pumping at the east edge of the profile. Flow through profile Section B-B' was modeled less satisfactorily by pumping at the profile edge. Relatively higher alluvium hydraulic conductivity values, and a somewhat reduced decline in the trend in water level were required to reasonably model subsidence in Section B-B'.

Two groundwater level scenarios were modeled to provide subsidence predictions to the year 2021. In a best-case scenario, the regional groundwater levels were assumed to remain relatively constant, as they have since the early 1990s as shown in Figure 6. In a presumed worst-case scenario, significant groundwater pumping in the western Salt River Valley is assumed to resume and groundwater levels are assumed to drop at a rate of 5 feet per year for a total drop of 100 feet between 2001 and 2021. The decline of 5 feet per year is approximately equal to the decline rate between the mid-1940s and the mid-1960s, as depicted in Figure 6.

It is probable that groundwater levels in the vicinity of the White Tanks mountain front were considerably higher during the Pleistocene compared to pre-development historic times. A cooler, wetter climate prevailed at that time, with the snow line elevation about 3000 feet lower across the earth compared to the present. At a comparative climatic elevation higher than 4600 feet above mean sea level, annual rainfall could have been closer to 20 inches than the present approximate 7 inches. Mountain front recharge would have been significantly greater than at present, particularly near the significant drainage just south of McMicken Dam. The resulting significantly higher groundwater elevations in the alluvium in the vicinity of the mountain front at the end of the Pleistocene may have slowly decayed through the current climate of the Holocene to the early historic levels before pumping, with resulting subsidence and horizontal ground strains occurring. This possible condition was modeled as a very slow 150-foot drop in groundwater level prior to the initial conditions assumed in 1947 to 1955 for the models. Results of this modeling are presented separately from the historic subsidence in various figures.

4.2.4 Survey and InSAR Subsidence Data

Survey results for the NGS survey line at the Beardsley Canal and crest elevation surveys for the dam that were used for the calibrations are presented in AMEC (2003). The dam crest elevation data are from the 2001 survey by the District (FCDMC, 2001) and the 1982 survey reported in Sergent, Hauskins & Beckwith (SHB, 1982). InSAR data provided by ADWR was further processed so that numeric elevation changes along various profiles could be obtained from the InSAR data (ADWR, 2003). This eliminated the need to manually interpret elevation changes based on color changes in the InSAR images.

5.0 SECTION A-A'

Section A-A' was important to modeling conditions leading to the development of both of the fissures identified in 1981 and the fissures identified in 2001. Considering the InSAR identified localized subsidence bowl (see Figure 1) and the possible complex interaction of both UAU and considerable FGU alluvium, this was the most complicated section to model. Modeling was performed assuming the elastic modulus of the alluvium changed over time as subsidence progressed, and assuming the elastic modulus of the alluvium remained constant through the subsidence process. When very similar answers resulted from both assumptions, further modeling of the other sections was performed using a constant modulus. The geologic model assumed for Section A-A' is presented in Figure 7. Calibrations and comparisons between modeled and measured subsidence for Section A-A' are presented in Figures 8, 10, 12 and 14. Modeled subsidence and subsidence predictions are presented in Figures 9 and 13, and modeled horizontal strains and strain predictions are presented in Figures 11 and 15. Figures 8 through 15 only include the western 6000 feet of the model shown in Figure 7, which is the area of interest to this study.

5.1 Section A-A' Profile

Section A-A' presented in Figure 7 closely approximates Figure 16 in AMEC (2003), the interpreted bedrock profile for a section oriented roughly east-southeast crossing the dam at about Station 57+00. This profile includes the bedrock high near the dam, the 2002 earth fissures at the dam, the 1981 fissures east of the dam and the InSAR interpreted subsidence bowl located east of the dam. The interpreted bedrock profile depth was based on interpretation of gravity data, with ReMi seismic reference depths at Lines L-7 and L-1 as presented in Figure 16 of AMEC (2003). Bedrock was interpreted to become deeper toward the east from the bedrock high, and then drop relatively rapidly near the east end of the profile, consistent with the presence of a basin-bounding fault. A possible middle fine-grained unit (MFGU) was assumed to be present below an elevation of about 600 feet to the east of the assumed basin bounding fault. The alluvium profile was interpreted as the upper alluvial unit (UAU), with a more clayey fine-grained unit (FGU) representing the InSAR interpreted subsidence bowl (see Figure 1) located east and southeast of the dam and earth fissures.

Subsidence was modeled to occur in the alluvium overlying bedrock. The bottom of the finite element mesh is at an elevation of 600 feet at the interpreted top of bedrock in the west portion of the profile, and the assumed top of the MFGU in the east portion of the profile. The finite element mesh represents a slice of the upper 750 feet of the basin over a distance of 9500 feet. The height of elements within the part of the mesh representing alluvium is 50 feet. The width of elements in the non-critical west and east edges of the model is 200 feet, transitioning to 100 feet at the bedrock high and within part of the FGU, and then becoming 50 feet in the critical

model areas associated with fissure zones. The bedrock and the bottom of the finite element mesh are modeled as no-flow boundaries. Where bedrock was deeper than the finite element mesh, the boundary condition was assumed to be the deeper MFGU.

The geometry of the clayey FGU was interpreted from the InSAR subsidence bowl with depth points along the profile referenced from Resistivity Sounding R-1, with the top of the FGU at a depth of 200 feet, and Resistivity Sounding R-4, with the top of the FGU at a depth of 140 feet. Historic water level measurements at Well 612994 located at Cactus Road and the Beardsley Canal also provide an indirect depth to the top of the FGU of about 350 feet. It was assumed that the well was drilled into the FGU, but having a total depth of only 534 feet, did not penetrate the FGU. Based on these data and the InSAR interpreted thickness, the lower bound of the FGU was interpreted to be at elevation 850 feet, as shown in Figure 7.

5.2 Section A-A' Calibration

Calibration for Section A-A' between 1947 and 1982 is presented in Figure 8, where the elastic modulus was varied as the subsidence conditions changed, and Figure 12 where the elastic modulus was assumed to remain constant. There was virtually no difference in the resulting modeled subsidence. Modeled subsidence was calibrated to two points, the actual subsidence measured by the crest survey at Station 55+00 on the dam (approximately zero subsidence) and the NGS survey at the nearest NGS monument along the Beardsley Canal. Subsidence was assumed to be negligible at locations west of the 1981 fissures. Along the profile between the 1981 fissures and the Beardsley Canal, subsidence was assumed to follow one of two trends. A straight-line trend (Observed (1) in Figure 8) from about zero feet of subsidence to about 2.7 feet at the canal resulted in strains insufficient to have caused the 1981 fissures. Another trend (Observed (2) in Figure 8) used the InSAR data (ADWR, 2003) to define a subsidence profile with a much sharper drop near the 1981 fissures and then a nearly level trend to the canal. This trend resulted in more credible horizontal strains at the location of the 1981 fissures.

Further Section A-A' model calibration compared the InSAR measured subsidence (ADWR, 2003) and modeled subsidence in the 1990s as presented in Figures 10 and 14. Lateral details of the modeled subsidence results as compared to InSAR data were mismatched by about 1,000 feet, but modeled subsidence magnitudes did match reasonably well. It should be noted that total modeled and measured subsidence through these time periods was in the range of only 0.08 to 0.23 feet.

5.3 Modeled Subsidence and Subsidence Predictions

Figures 9 and 13 present modeled subsidence for several time periods ranging from 1947 to 1999, and predicted subsidence to 2021. The modeled subsidence clearly shows a decrease in subsidence rate from before 1981 to the present rate. Predicted subsidence in 2021 under present groundwater conditions may be an additional 0.5 feet in the maximum subsidence area, and still be very small in the vicinity of the dam. If resumed pumping drops the groundwater table an additional 100 feet by 2021, the resulting maximum additional subsidence may be about 1 foot from present elevations. The subsidence rate increases most rapidly near the 1981 fissures, and also increases near the 2002 fissures.

The modeled prehistoric subsidence presented in Figure 13, which might reasonably represent subsidence since the last Ice Age, has maximum values similar to the historic subsidence. However, the subsidence rate increases most rapidly near the 2002 fissures. If fissures were to develop, they would develop near the 2002 fissures. The 1981 fissures are in an area where fissure development would not be anticipated. This modeled difference in fissure location likely is due to the time delay effects of the FGU. At very slow geologic rates of groundwater level drop, the FGU has sufficient time to drain groundwater out of the alluvium in spite of its very low hydraulic conductivity. Thus, the differences in hydraulic conductivity of the FGU and UAU alluvium are less likely to set up localized differential subsidence in the basin alluvium. At very rapid rates of groundwater level drops, the differences in hydraulic conductivity between the FGU and UAU result in a very different pattern in the differential subsidence across the profile.

5.4 Modeled Horizontal Strain and Horizontal Strain Predictions

Figures 11 and 15 present the modeled horizontal strain for several time periods ranging from 1947 to 1999, and for predictions to 2021. The modeled strain clearly shows that strain had exceeded the approximate strain threshold of 0.02 percent by 1981 in the area of the 1981 fissures, and is predicted to have been about 0.04 percent. In the area of the 2002 fissures, predicted strain was slightly greater than 0.02 percent. A decrease in strain rate from before 1981 to the present rate was modeled. The vicinity of the 1981 and 2002 fissures were the only areas in the model where strains were significantly tensile, and the fissures were located at local peaks in the tensile strain. Predicted tensile strain in 2021 under present groundwater conditions was modeled to be little changed at the location of the 1981 fissures and only slightly higher at the location of the 2002 fissures. If resumed pumping drops the groundwater table an additional 100 feet by 2021, the resulting tensile strains would be slightly increased and still be in the same profile area.

The modeled prehistoric subsidence presented in Figure 15, which might reasonably represent horizontal strain since the last Ice Age, has a sharp, narrow zone of tensile strain at the location of the 2002 fissures. This is consistent with the predicted subsidence profile in Figure 13.

Strain at the location of the 2002 fissures was modeled to be about 0.06 percent. However, it is anticipated that the rate of strain was very slow, occurring perhaps over thousands of years, rather than the tens of years for modern fissuring. Thus, even though modeled historic strains at the location of the 2002 fissures are only slightly higher than 0.02 percent, the ground at that location may have been placed into significant tension and perhaps even cracked in prehistoric times.

6.0 SECTION B-B'

Section B-B' in Figure 16 encompasses the length of McMicken Dam where mitigation of earth fissures is required. The model shown in Figure 16 is essentially the same as the model shown in Figure 17 in AMEC (2003). Section B-B' represents the section of McMicken Dam requiring further analysis of horizontal strains because of the presence of earth fissures near Station 65+00. Based on the studies presented in AMEC (2003), the high fissure hazard zone was determined to extend to Station 75+00, and the moderate fissure hazard zone was determined to extend from Station 75+00 to Station 105+00 (see Figure 1). The analyses presented herein were completed to further refine the fissure hazard zone delineation along the McMicken Dam axis.

The successful modeling of Section A-A' included a reasonable explanation for the presence of the 2002 earth fissures. Section B-B' also had to be consistent with the presence of the 2002 fissures, and with the essential basin alluvium material properties used to successfully model Section A-A'. Because Section B-B' is sub-perpendicular to assumed basin groundwater flow, higher hydraulic conductivity values were required to be assumed for the upper alluvium to reasonably model the groundwater flow. This is because the model utilized pumping at the northeast edge of the profile to induce the drop in the groundwater level.

The geologic models for Section B-B', which extends from Station 40+00 to Station 160+00, are presented in Figures 16 and 18. Calibrations and comparisons between modeled and measured subsidence for Section B-B' are presented in Figures 17, 19 and 20. Modeled subsidence and subsidence predictions are presented in Figure 21, and modeled horizontal strains and strain predictions are presented in Figure 22. Figures 17 and 19 through 22 do not extend the full length of the model shown in Figures 16 and 18, since only relevant results of the modeling effort are presented.

6.1 Section B-B' Profile

The initial Section B-B' profile along McMicken Dam from Stations 40+00 to 120+00 presented in Figure 16 matched that presented as Figure 17 in AMEC (2003), which interpreted the bedrock profile oriented in a roughly southwest-northeast direction. This profile included the bedrock high at the south end of the dam, the 2002 earth fissure features at the dam and InSAR

interpreted subsidence extending north from the subsidence bowl shown in Figure 1. The interpreted bedrock profile depth was based on gravity interpretation and ReMi seismic reference depths. However, a lens of FGU alluvium had not been included in the original gravity interpretation, and the first subsidence calibration attempt was not successful. After the successful modeling of Section A-A' including the FGU, it was apparent that the gravity model needed to be updated. A new Section B-B', presented in Figure 18, was developed. Based on the calibration of Section A-A', an FGU section was added to the upper alluvium and the gravity interpretation of the bedrock contact was revised.

6.2 Section B-B' Calibration

The initial Section B-B' calibration between 1955 and 1982 is presented in Figure 17, where subsidence was modeled using the bedrock contact presented in Figure 16 from AMEC (2003). Modeled subsidence was compared in Figure 17 to changes in dam crest elevation based on initial construction height and the 1982 survey (SHB, 1982). There was an unexplained condition in this data set between Stations 40+00 and 60+00 where the 1982 elevation appeared to rise upward before dropping rapidly at about Station 65+00. To avoid this data quality issue, there was assumed to be zero subsidence rather than ground rise south of Station 65+00. The initial profile modeled insufficient change in subsidence rate in the area of the 2002 fissures. Furthermore, considerable change in subsidence rate was modeled beginning at about Station 80+00 where no evidence of fissuring has been observed to date.

A new Section B-B' profile, as shown in Figure 18, was developed and interpreted. The addition of the FGU reduced the density of the alluvium so that the bedrock contact modeled in the northern portion of the profile generally underlying the FGU was not as deep as the initial profile. This new Section B-B' calibration between 1955 and 1982 is presented in Figure 19. With the new profile, a significant change in subsidence rate occurs at about Station 55+00, and the modeled and measured subsidence north of about Station 80+00 are very closely matched. This profile indicates fissuring as most likely occurring about 500 to 1,000 feet south of the observed fissure features. However, as shown in Figure 20, modeled subsidence between 1985 and 2001 matches the location of the significant subsidence rate change as determined by survey between about Stations 56+00 and 60+00 (FCDMC, 2001). If better deep subsurface information becomes available in the future, the profile might be able to be modeled more precisely.

Further Section B-B' model calibration compared the InSAR measured subsidence (ADWR, 2003) and modeled subsidence from 1992 to 1999, as presented in Figure 20. Lateral details of the modeled subsidence compare reasonably with the InSAR data, but modeled subsidence magnitudes were considerably higher in the vicinity of Station 117+50. It should be noted that the total modeled and measured subsidence since 1985 or 1992 was in the range of only about 0.1 to 0.9 feet, likely approaching the limits of the analysis method.

6.3 Modeled Subsidence and Subsidence Predictions

Figure 21 presents the modeled subsidence for several time periods ranging from 1955 to 2001 and predictions to 2021. The modeled subsidence clearly shows a decrease in subsidence rate from before 1981 to the present rate. Predicted subsidence in 2021 under present groundwater conditions may be an approximate additional 0.4 feet in the maximum subsidence area in the vicinity of Stations 110+00 to 120+00. If resumed pumping drops the groundwater table an additional 100 feet by 2021, the resulting maximum additional subsidence may be roughly about 1.7 feet from present elevations. The subsidence rate increases most rapidly near the 2002 fissure features.

The modeled prehistoric subsidence presented in Figure 21, which might reasonably represent subsidence since the last Ice Age, has maximum values nearly twice the historic subsidence. However, the subsidence rate increases most rapidly near the 2002 fissures. If fissures were to have developed, they would have developed near the 2002 fissures. The presence of the FGU appears to have less localized influence in Section B-B' compared to Section A-A'.

6.4 Modeled Horizontal Strain and Horizontal Strain Predictions

Figure 22 presents the modeled horizontal strain for several time periods ranging from 1955 to 2001 and predictions to 2021. The modeled strain clearly shows that strain had exceeded the approximate strain threshold of 0.02 percent by 1981 in the area of the 2002 fissure features, and is predicted to have been about 0.03 percent. A decrease in strain rate from before 1981 to the present rate was modeled, but by 2002 the tensile strain at the features is predicted to have reached about 0.04 percent. To the present time, the vicinity of the 2002 fissure features were the only areas in the model where strains were significantly tensile and had exceeded 0.02 percent. The model indicated that the predicted tensile strain in 2021 under present groundwater conditions will be changed very little at the location of the 2002 fissure features. If resumed pumping drops the groundwater table an additional 100 feet by 2021, the resulting tensile strains would be increased to about 0.04 percent at the features, and could slightly exceed 0.02 percent at about Station 80+00. Station 95+00 is another location with modeled tensile strain that almost reaches 0.02 percent by 2001, but then appears to decay somewhat in the future.

The modeled prehistoric subsidence presented in Figure 22, which might reasonably represent horizontal strain since the last Ice Age, has a sharp, narrow zone of tensile strain near the location of the 2002 fissure features. This is consistent with the predicted subsidence profile in Figure 21. Tensile strain near the 2002 fissure features location and at about Station 95+00 was modeled to be about 0.04 percent. However, it is anticipated that the rate of strain was

very slow, occurring perhaps over thousands of years rather than the tens of years for modern fissuring. Thus, the ground at and near the 2002 fissure features may have been placed into significant tension and perhaps even cracked in prehistoric times.

7.0 SECTION C-C'

Section C-C' is a west-east profile at dam Station 65+00 near the location of the 2002 fissure features at the dam. The successful modeling of Sections A-A' and B-B' included a reasonable explanation for the presence of the 2002 earth fissure features. Section C-C' also had to be consistent with the presence of the 2002 fissures and with the essential basin alluvium material properties used to successfully model Section A-A'. Because Section C-C' was sub-parallel to the assumed basin groundwater flow direction and to Section A-A', model permeability values in the upper alluvium were similar to those in Section A-A'.

The geologic model for Section C-C' is 9000 feet in length as shown in Figure 23. Calibrations and comparisons between modeled and measured subsidence for Section C-C' are presented in Figures 24 and 25. Modeled subsidence and subsidence predictions are presented in Figure 26, and modeled horizontal strain and strain predictions are presented in Figure 27. Figures 24 through 27 do not extend the full length of the model shown in Figure 23 since only relevant results of the modeling effort are presented.

7.1 Section C-C' Profile

Section C-C' utilized a profile interpolated between Section A-A' and Section B-B', as shown in Figure 23. Again, the upper alluvium included a FGU zone dimensioned according to the InSAR results presented in Figure 1. However, little other control was available to improve on bedrock depths beyond interpolation from the other profiles.

7.2 Section C-C' Calibration

Section C-C' calibration between 1947 and 1981 is presented in Figure 24. Similar to Section A-A', modeled subsidence was calibrated to actual subsidence measured by survey (FCDMC, 2001) at Station 65+00 on the dam and at the nearest NGS monument along the Beardsley Canal. Subsidence west of the 2002 fissure features at about grid distance 1,000 was assumed to be negligible. Along the profile between the 2002 fissure features and the Beardsley Canal, subsidence was assumed to follow a straight-line trend from about zero feet subsidence to about 2.7 feet at the canal. InSAR data (ADWR, 2003) indicated that this was a reasonable assumption.

Further Section C-C' model calibration compared the InSAR measured subsidence (ADWR, 2003) and modeled subsidence in the 1990's as presented in Figure 25. Lateral details of the modeled subsidence versus InSAR results were mismatched by about 1,000 feet, but modeled subsidence magnitudes did match reasonably well. It should be noted that total modeled and measured subsidence through these time periods was in the range of only 0.07 to 0.22 feet, which is probably at or beyond the accuracy limits of the modeling procedures.

7.3 Modeled Subsidence and Subsidence Predictions

Figure 26 presents the modeled subsidence for several time periods ranging from 1947 to 2001 and predictions to 2021. The modeled subsidence clearly shows a decrease in subsidence rate from before 1981 to the present rate. Predicted subsidence in 2021 under present groundwater conditions may be an approximate additional 0.4 feet. If resumed pumping drops the groundwater table an additional 100 feet by 2021, the resulting maximum additional subsidence may be about 0.7 feet from present elevations. The subsidence increases most rapidly near the location of the 2002 fissure features (grid distance of about 1200 feet).

The modeled prehistoric subsidence presented in Figure 26, which might reasonably represent subsidence since the last Ice Age, has maximum values almost three times the historic subsidence. However, the subsidence rate increases most rapidly near the location of the 2002 fissures. If fissures were to have developed, they would have developed near the 2002 fissures. The presence of the FGU appears to have less localized influence in Section C-C' as compared to Section A-A'.

7.4 Modeled Horizontal Strain and Horizontal Strain Predictions

Figure 27 presents the modeled horizontal strain for several time periods ranging from 1947 to 2001 and predictions to 2021. The modeled strain clearly shows that strain had exceeded the approximate strain threshold of 0.02 percent by 1981 in the area of the 2002 fissure features and is predicted to have been about 0.025 percent. A decrease in strain rate from before 1981 to the present rate was modeled, but by 2001 the tensile strain at the features was predicted to have reached about 0.03 percent. To the present time, the vicinity of the 2002 fissure features is the only area in the model where strains were significantly tensile and had exceeded 0.02 percent. Tensile strain in 2021 under present groundwater conditions was predicted to not change significantly at the location of the 2002 fissure features. If resumed pumping drops the groundwater table an additional 100 feet by 2021, the resulting tensile strains would be increased to about 0.033 percent at the features.

The modeled prehistoric subsidence presented in Figure 27, which might reasonably represent horizontal strain since the last Ice Age, has a sharp, narrow zone of tensile strain near the location of the 2002 fissure features. This is consistent with the predicted subsidence profile in Figure 26. Tensile strain near the 2002 fissure features location and at about Station 95+00 was modeled to be about 0.10 percent. However, it is anticipated that the rate of strain was very slow, occurring perhaps over thousands of years rather than the tens of years for modern fissuring. Thus, the ground at and near the 2002 fissure features may have been placed into significant tension and perhaps even cracked in prehistoric times.

8.0 SECTION D-D'

Section D-D' is a southwest-northeast profile at dam Station 65+00 at the location of the 2002 fissure features at the dam. This section was oriented to attempt to be perpendicular to the 2002 fissure features. It is very similar to Section C-C'.

The geologic model for Section D-D' is 7500 feet in length as shown in Figure 28. Calibrations and comparisons between modeled and measured subsidence for Section D-D' are presented in Figure 29. Modeled subsidence and subsidence predictions are presented in Figure 30, and modeled horizontal strain and strain predictions are presented in Figure 31. Figures 29 through 31 do not extend the full length of the model shown in Figure 28 since only relevant results of the modeling effort are presented. Also the zero distance on Figures 29 through 31 corresponds to the zero distance on Figure 28.

8.1 Section D-D' Profile

The Section D-D' profile presented in Figure 28 is very similar to the Section C-C' profile. Again, the upper alluvium included a FGU zone dimensioned according to the InSAR results presented in Figure 1. However, little other control was available to improve on bedrock depths beyond interpolation from the other profiles.

8.2 Section D-D' Calibration

Section D-D' calibration was nearly identical to the Section C-C' calibration between 1947 and 1981 as presented in Figure 24. Further Section D-D' model calibration compared the InSAR measured subsidence (ADWR, 2003) and modeled subsidence in the 1990s as presented in Figure 29. Lateral details of the modeled subsidence versus the InSAR results did not match very well at the low magnitudes of subsidence of about 0.07 to 0.15 feet through these time periods. However, effects from these subsidence magnitudes due to secondary compression in the FGU were very small compared to the large subsidence that occurred during periods of significant groundwater table drop prior to 1981.

8.3 Modeled Subsidence and Subsidence Predictions

Figure 30 presents the modeled subsidence for several time periods ranging from 1947 to 2001 and predictions to 2021. The modeled subsidence clearly shows a decrease in subsidence rate from before 1981 to the present rate. Predicted subsidence in 2021 under present groundwater conditions may be an approximate additional 0.1 to 0.2 feet. If resumed pumping drops the groundwater table an additional 100 feet by 2021, the resulting maximum additional subsidence may be roughly about 0.8 to 1.0 feet from present elevations.

8.4 Modeled Horizontal Strain and Horizontal Strain Predictions

Figure 31 presents the modeled horizontal strain for several time periods ranging from 1947 to 2001 and predictions to 2021. The modeled strain shows that tensile strain reached the approximate strain threshold of 0.02 percent by 1999 only at a location about 3,200 feet along the profile. Under future scenarios through 2021, tensile strain is not predicted to increase further at this location. Strains in the vicinity of the trend of the 2002 fissure features at a distance of about 800 feet along the profile were less than 0.02 percent by 1999. Tensile strains predicted by the model in 2021 under the present groundwater conditions were changed very little along the trend of the 2002 fissures. If resumed pumping drops the groundwater table an additional 100 feet by 2021, the resulting tensile strains along the trend of the 2002 fissures would be increased to about 0.02 percent.

The modeled prehistoric subsidence presented in Figure 31, which might reasonably represent horizontal strain since the last Ice Age, has a sharp, narrow zone of tensile strain at about distance 3,200 feet along the profile. The model determined a maximum tensile strain at this location of about 0.05 percent. This is consistent with the predicted subsidence profile in Figure 30. However, it is anticipated that the rate of strain was very slow, occurring perhaps over thousands of years rather than the tens of years for modern fissuring. Furthermore, prehistoric strain in the vicinity of the trend of the 2002 fissures is modeled as having been compressive rather than tensile.

9.0 DISCUSSION AND CONCLUSIONS

In general, the numerical analyses confirmed the previously determined boundaries of the high fissure risk zone at the south end of the dam, based on horizontal strains in excess of the threshold 0.02 percent strain being developed by the time of the field investigations completed in 1981 and in late 2002. Analyses of sections within the moderate fissure risk zone calculated horizontal strains approaching, but not exceeding, the threshold horizontal strain, generally confirming the boundaries of this zone. The modeled horizontal strain at the locations of the 1981 and 2002 earth fissures can be summarized as follows:

- A maximum horizontal tensile strain of slightly more than 0.04 percent in 1981 was estimated for the location of the 1981 earth fissures along Section A-A' as shown in Figures 11 and 12. In the model, horizontal strains to the east of this location were compressive.
- A maximum horizontal tensile strain of slightly more than 0.03 percent in 1999 was estimated for the location of the 2002 earth fissures along Section A-A', as shown in Figures 11 and 12. In the model, the horizontal strain at the location of the 1981 earth fissures had increased to about 0.05 percent by 1999. These tensile strains are consistent with these locations being in the high fissure risk zone. Horizontal strains to the east of the location of the 1981 earth fissures were compressive, consistent with the eastern boundary of the high fissure hazard zone.
- A maximum tensile horizontal strain of about 0.03 percent in 1981 was estimated for Station 57+50, south of but very near the location of the 2002 earth fissures, as shown in Figure 22. In the model, the horizontal strain increased to about 0.045 percent by 2001. These tensile horizontal strains are consistent with this location being in the high fissure risk zone.
- Tensile horizontal strains further north along McMicken Dam also were tensile, being about 0.015 percent near Station 81+00 and almost 0.02 percent near Station 95+00, as shown in Figure 22. These horizontal strains are consistent with these locations being within the moderate fissure risk zone, rather than the high fissure risk zone.
- The zone of tensile horizontal strain along the south end of McMicken Dam extends from about Station 62+00 to about Station 45+00, thus the southern boundary of the high fissure risk zone may extend further south than Station 55+00 as previously estimated. Based on the model results presented in Figure 22, the zone possibly could extend to Station 50+00. This does not impact the current design for the rehabilitation of the dam.
- A maximum tensile horizontal strain of about 0.025 percent in 1981 was estimated for a location about 250 feet northeast of Station 65+00, increasing to about 0.03 percent in 1999, as shown in Figure 27. Horizontal strains further to the east were compressive. Thus, the model predicted a lesser lateral extent of the high fissure risk zone than previously determined.
- A maximum tensile horizontal strain of about 0.01 percent in 1981 was estimated for Station 65+00, the location of the 2002 fissure, increasing only slightly by 1999, as shown in Figure 31. This is not consistent with the location of the high fissure risk zone, since the threshold horizontal strain of 0.02 percent is not attained.

- A maximum tensile horizontal strain of almost 0.02 percent in 1981 was estimated for a location northeast of McMicken Dam in the moderate fissure risk zone (location 3200 feet on Section D-D'), increasing only slightly to 0.02 percent by 1999, as shown in Figure 31. This is consistent with moderate fissure hazard zone.

The analyses also indicate the degree of risk will vary depending on future groundwater pumping. If groundwater levels remain stable, the risk will remain essentially the same, with the amount of horizontal tensile strain at the locations remaining the same or increasing only slightly. In some cases, the width of the zone of tensile stress also increases slightly (see Figure 16, for example). However, if groundwater levels drop significantly (on the order of the 100 feet assumed by 2021), the risk will be intensified, with additional subsidence and horizontal strain development. For example, as shown in Figure 22, the maximum tensile horizontal strain at about Stations 81+00 and 95+00 approach or slightly exceed the threshold value of 0.02 percent. However, the areas where tensile horizontal strain exceeds the threshold value of 0.02 percent do not widen significantly.

Review of the basis of the analyses, including the assumptions required for development of the geologic profiles and the assumed materials parameters, led to the conclusion that the technological limits of the analyses had been reached. For example, the properties and geometry of the continuous alluvium were simplified in the geologic models as two or three units (UAU, FGU and/or MFGU). In actuality, a range of materials with varying properties would be present within these units, but cannot be differentiated based on the available or technically obtainable information. Similarly, fine details of the geometric distribution of the materials cannot be quantified, much less modeled, based on available or technically obtainable information. Thus, though the modeling effort determined some inconsistencies with the locations of the high and moderate fissure risk zones, these are not significant enough to alter their defined locations. Further, the results of the modeling effort do not require a change in the mitigation approach to McMicken Dam developed based on the location of the high and moderate fissure risk zones.

Flood Control District of Maricopa County
Final Zoning of Earth Fissure Risk & Determination
of Part(s) of the Dam that Require Dam Safety Modifications
McMicken Dam Fissure Risk Zone Remediation Project
Contract FCD 2002C011, Work Assignment No. 2A
AMEC Job No. 2-117-001066
5 November 2003

REFERENCES

AMEC Earth & Environmental, Inc., 2003, Earth Fissure Investigation Report, McMicken Dam, Work Assignment Nos. 4 & 5, Contract FCD 2000C006, Maricopa County, 11 April.

Arizona Department of Water Resources (ADWR), 2003, file 920918_990524_2439_vv_McMicken .txt, last modified 02/13/2003, 4:40 am, provided by Maurice A. Tatlow.

Bell, J.W., F. Amelung, A.R. Ramelli, and G. Blewitt, 2002, Land Subsidence in Las Vegas, Nevada 1935-2000: New Geodetic Data Show Evolution, Revised Spatial Patterns and Reduced Rates, Environmental and Engineering Science, Vol. 7, No.3, p. 155-174.

Boling, J.K., Carpenter, M.C., Johnson, N.M., and Davis, S.N., 1980, Measurements, Prediction and Hazard Evaluation of Earth Fissures and Subsidence, South Central Arizona, OWRT Project No. A-092-Ariz, The University of Arizona, Tucson.

Carpenter, M. C. 1993. Earth-Fissure Movements Associated with Fluctuations in Ground-Water Levels near the Picacho Mountains, South-Central Arizona, 1980-84. U. S. Geological Survey Professional Paper 497-H. Washington: U. S. Government Printing Office.

Geo-Slope International Ltd., 1998, Slope Stability Computer Program SLOPE/W, Version 4, Calgary, Alberta, Canada.

Flood Control District of Maricopa County, 2001, McMicken Dam, Subsidence Survey Data Review, October 31.

Haneberg, W.C., 1992. Drap Folding of Compressible Elastic Layers, I. Analytical Solutions for Vertical Uplift, Journal of Structural Geology, Vol. 14, No. 6, p. 713-721.

Holzer, T.L., Davis, S.N., and Lofgren, B.E., 1979, Faulting Caused by Groundwater Extraction in South Central Arizona, Journal of Geophysical Research, Vol. 84, No. B2, p.603-612.

Hoffmann, J., D.L. Galloway, H.A. Zebker and F. Amelug, 2001. Seasonal Subsidence and Rebound in Las Vegas Valley, Nevada, Observed by Synthetic Aperture Radar Interferometry, Water Resource Research, Vol. 37, p. 1551-1566.

Hoffmann, J., D.L. Galloway, H.A. Zebker , 2003. Inverse Modeling of Interbed Storage Parameters using Land Subsidence Observations, Antelope Valley California, Water Resource Research, Vol. 39, No. 2, p. 1-13.

Hirose, K., Y. Maruyama, D. Murdohardono, A. Effendi, H.Z. Abidin, 2001. Land Subsidence Detection using JERS-1 SARS Interferometry, 22nd Asian Conference on Remote Sensing, Singapore, November 5-9.

Jachens, R.C. and Holzer, T.L., 1982. Differential Compaction Mechanism for Earth Fissures near Casa Grande, Arizona, Geological Society of America Bulletin, Vol. 93, p. 998-1012.

Leake, S.A., 1991. Simulation of vertical computation in models of regional ground-water flow, in Johnson, A.I., ed., Land Subsidence: International Symposium on Land Subsidence, 14th, May 1991, Houston, Texas, International Association of Hydrological Sciences Publication 200, p. 565-574.

Leake, S.A., and P.A. Hsieh, 1995. Simulation of Deformation of Sediments from Decline of Groundwater Levels in an Aquifer Underlain by a Bedrock Step, USGS Subsidence Interest Group Conference, Proceedings of Technical Meeting, Las Vegas, Nevada, February 14-16, USGS Survey Open-File Report 97-47.

Lee, K.L. and Shen, C.K., 1969, Horizontal movements related to subsidence, Journal of the Soil Mechanics and Foundation Division, Proceedings of the American Society of Civil engineers, No. 95, SM1, January, pp. 139-166.

Schumann, H.H., 1992. Land Subsidence and Earth Fissure Hazards near Luke Air Force Base, Arizona. USGS Subsidence Interest Group Conference, Edwards AFB, Antelope Valley, Nov. 18-19. USGS Survey Open-File Report 94-532.

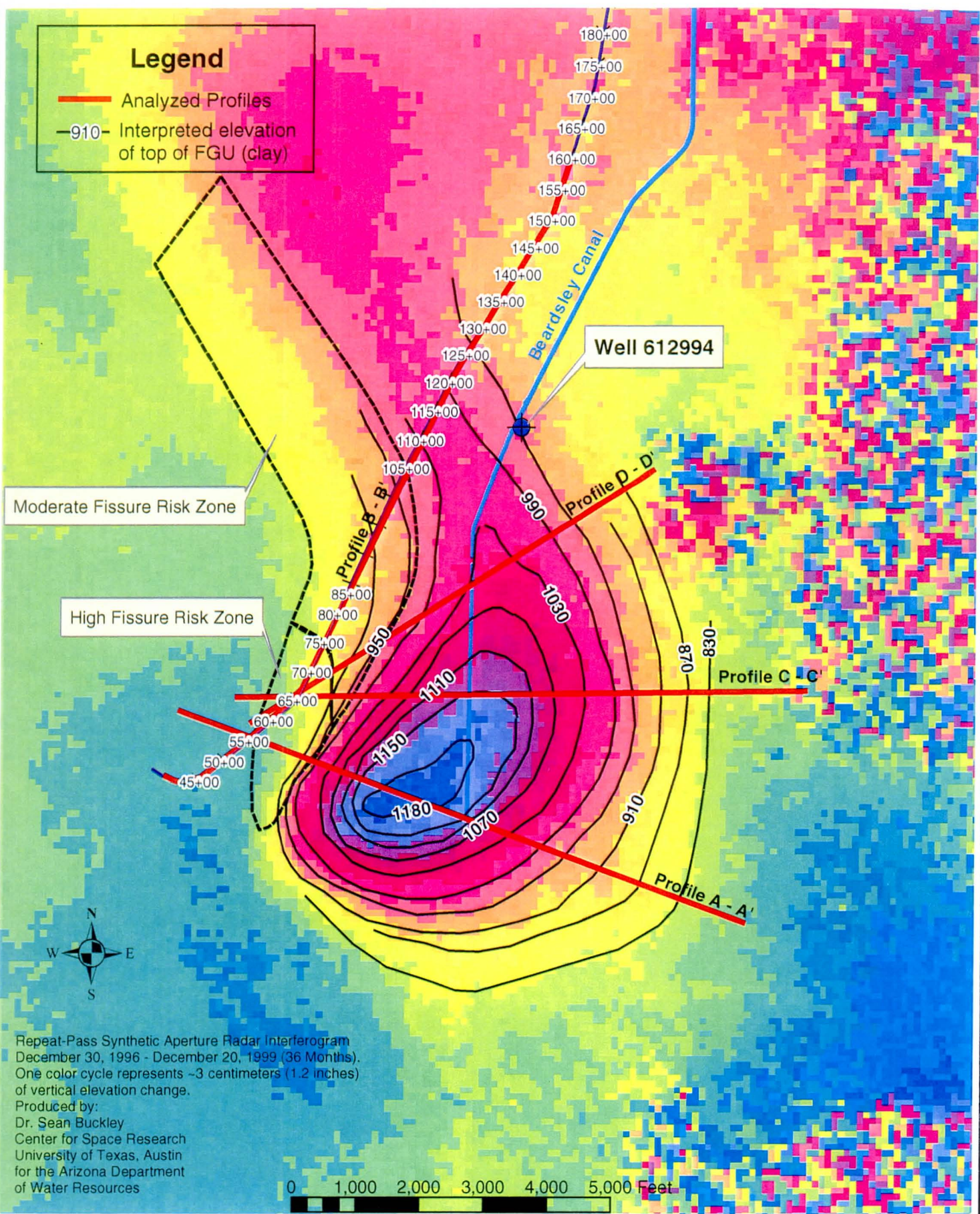
Sergent, Hauskins & Beckwith (SHB), 1982, Geotechnical Investigation Report, McMicken Dam Restoration Study, Maricopa County, Arizona, SHB Job No. E81-138, Phase II, July 27.

USGS Circular 1182, 1999. Land Subsidence in the United States, 177p.

FIGURES

Legend

- Analyzed Profiles
- 910- Interpreted elevation of top of FGU (clay)



JOB NO.:	2-117-001066
DESIGN:	MLR
DRAWN:	EMP
DATE:	10/1/03
SCALE:	1:24,000

McMicken Dam Fissure Risk Zone Remediation Project
 Contract FCD 2002C011
 Maricopa County, Arizona

SITE PLAN WITH CONCEPTUAL
 INTERPRETED FGU (CLAY) ELEVATION

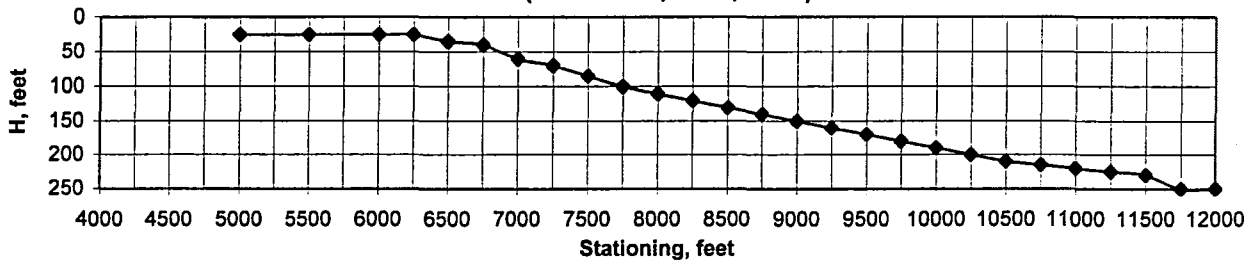
FIGURE
1



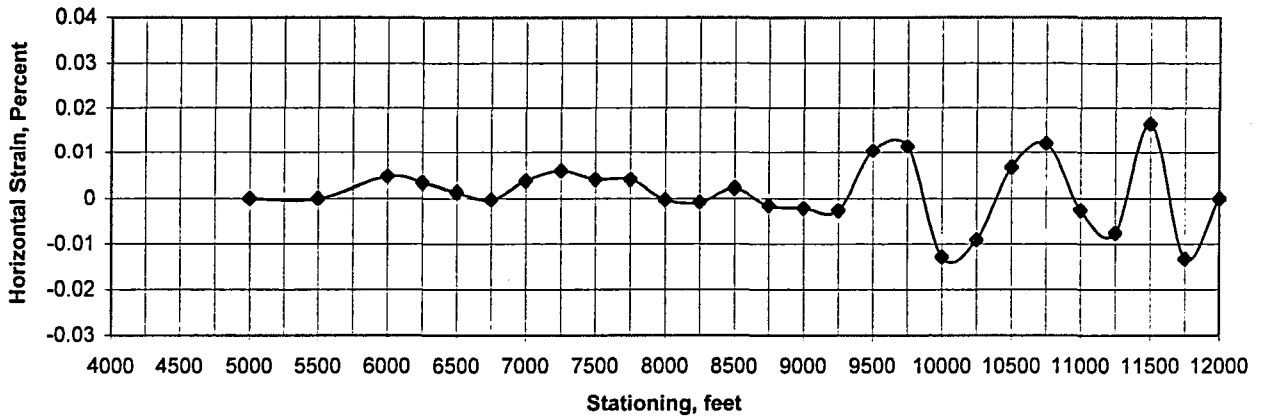
Ma 11/03/2003 1:36:29 PM
 ering I
 antu20C
 . its2-11
 i6 McV
 am Fis
 : Zone
 /_Interf
 -96-99

Figure 2 Lee and Shen Analysis - McMicken Dam

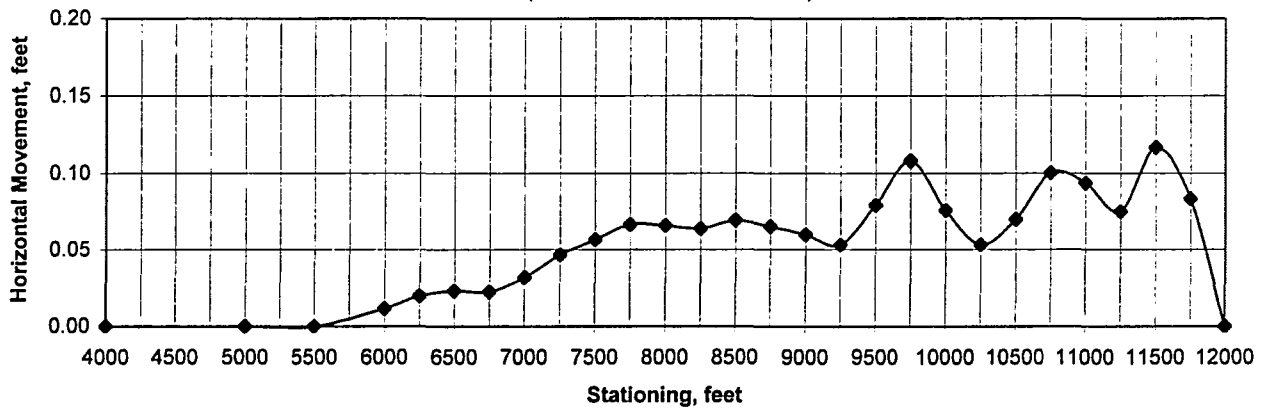
Section B-B' (1955-1982; SHB, 1982) CASE X-1



Section B-B' (1955-1982; SHB, 1982) CASE X-1



Section B-B' (1955-1982; SHB, 1982) CASE X-1



Section B-B' (1955-1982; SHB, 1982) CASE X-1

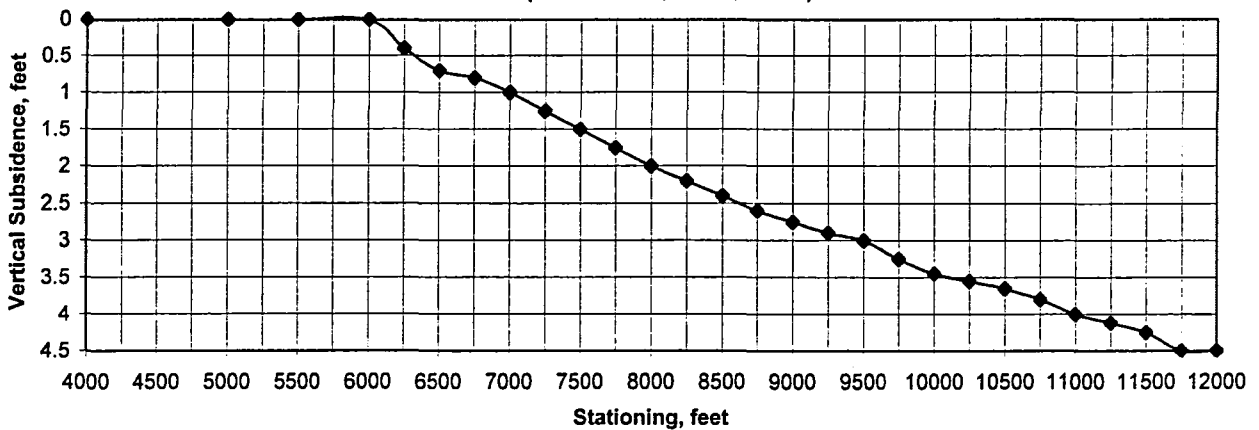
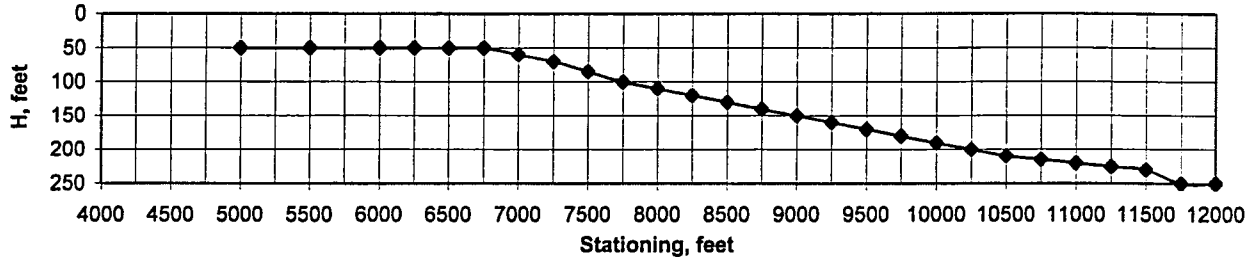


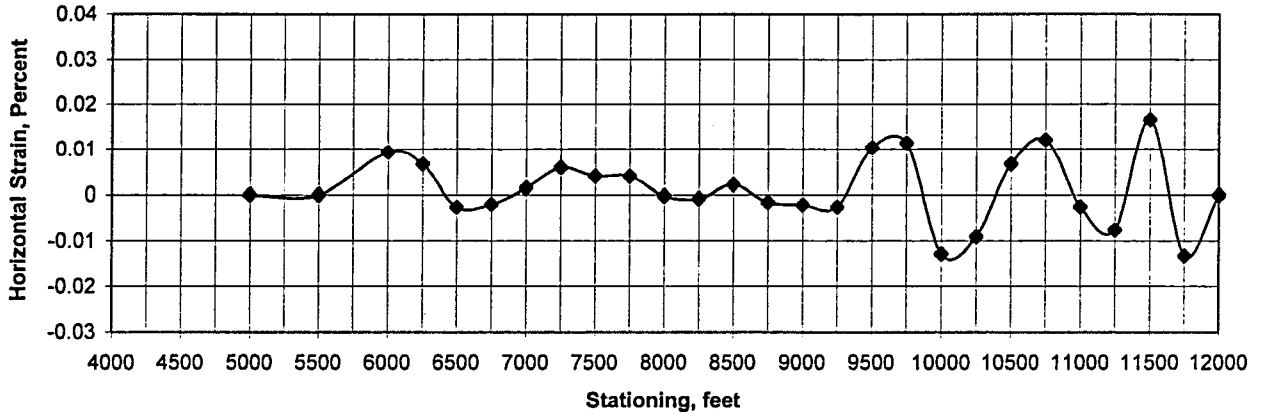
Figure 3

Lee and Shen Analysis - McMicken Dam

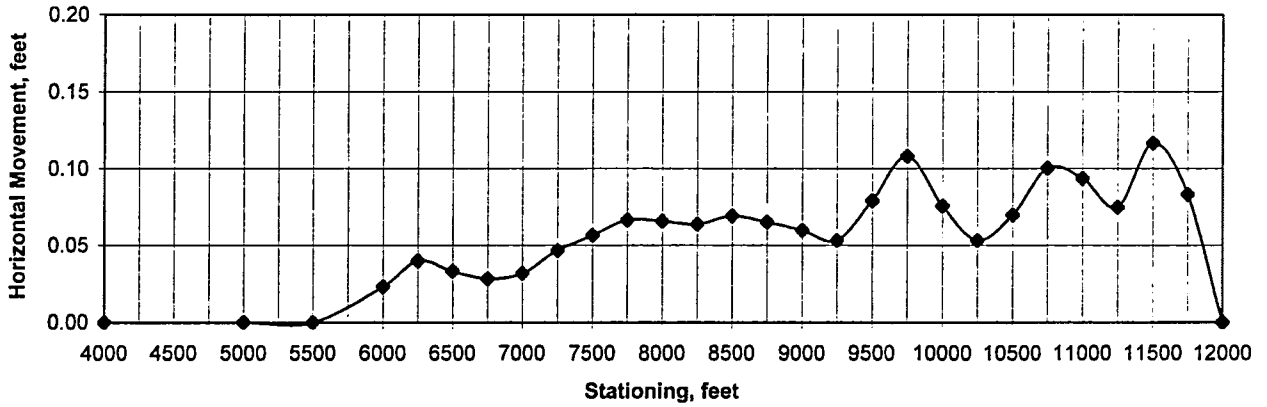
Section B-B' (1955-1982; SHB, 1982) CASE X-2



Section B-B' (1955-1982; SHB, 1982) CASE X-2



Section B-B' (1955-1982; SHB, 1982) CASE X-2



Section B-B' (1955-1982; SHB, 1982) CASE X-2

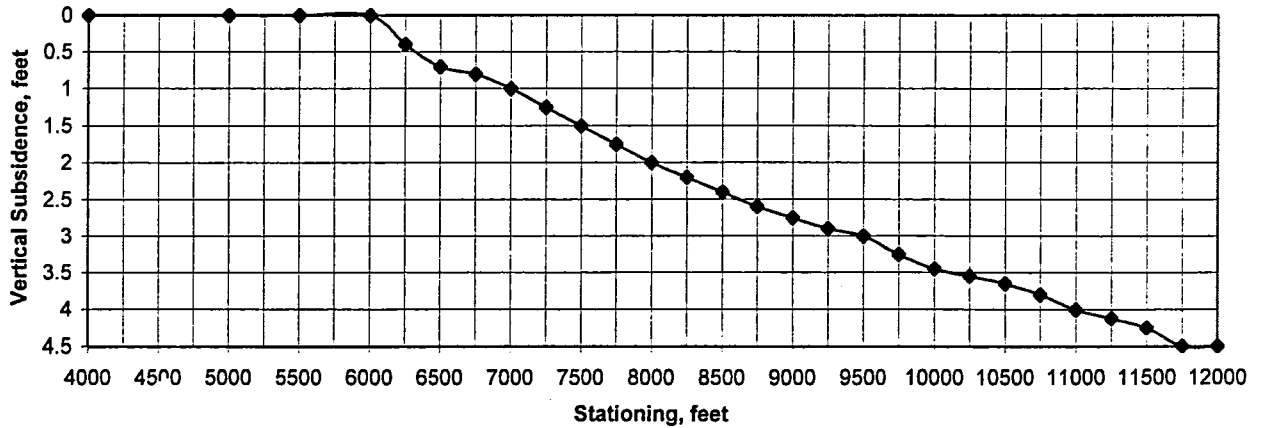
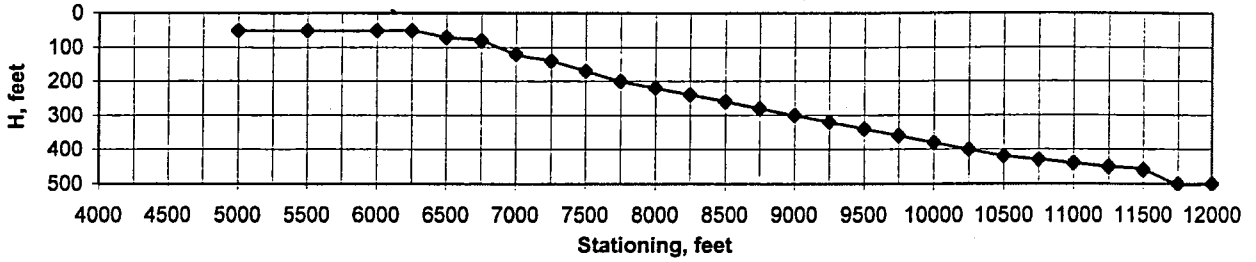


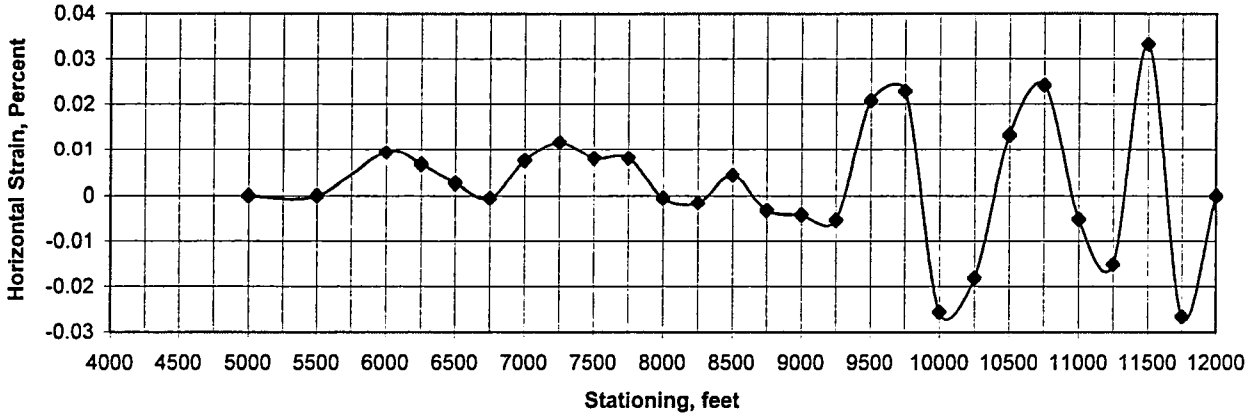
Figure 4

Lee and Shen Analysis - McMicken Dam

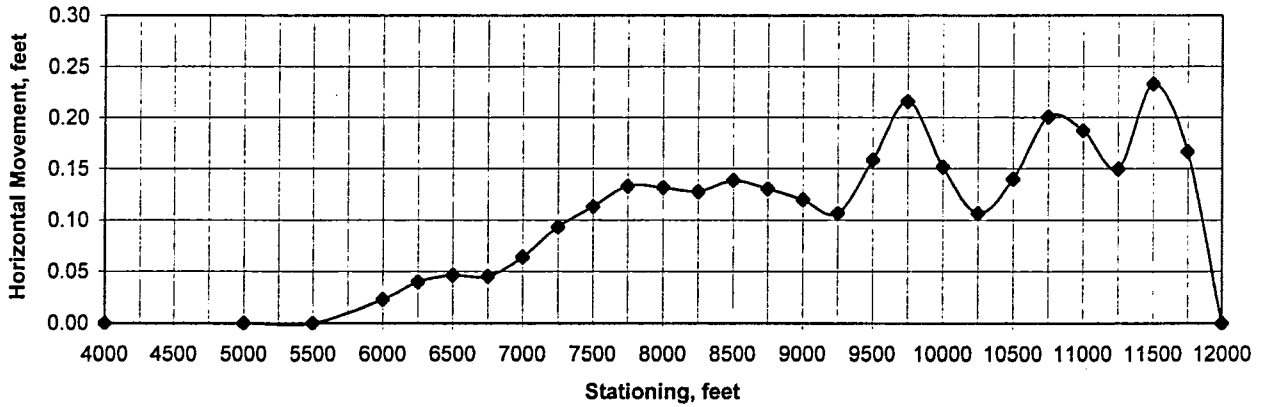
Section B-B' (1955-1982; SHB, 1982) CASE Y-1



Section B-B' (1955-1982; SHB, 1982) CASE Y-1



Section B-B' (1955-1982; SHB, 1982) CASE Y-1



Section B-B' (1955-1982; SHB, 1982) CASE Y-1

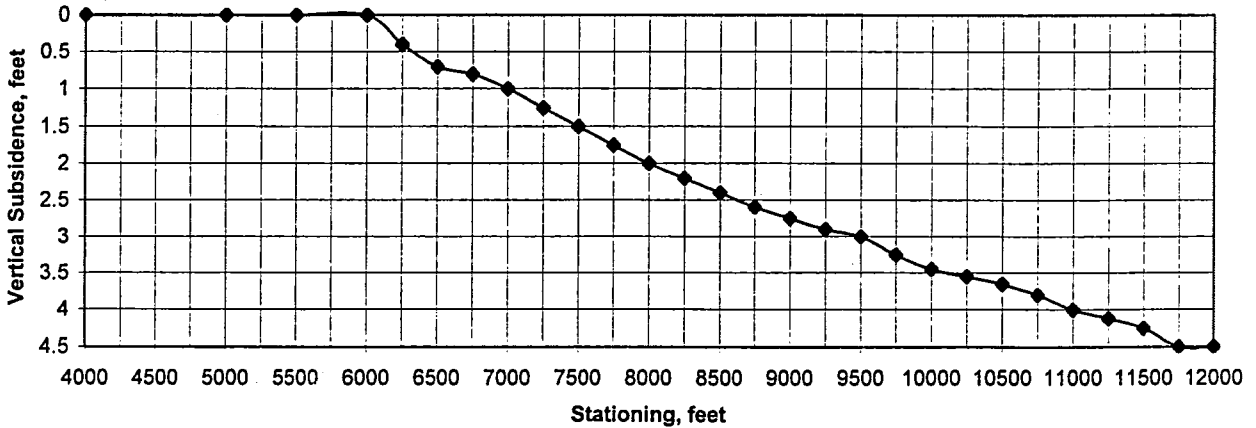
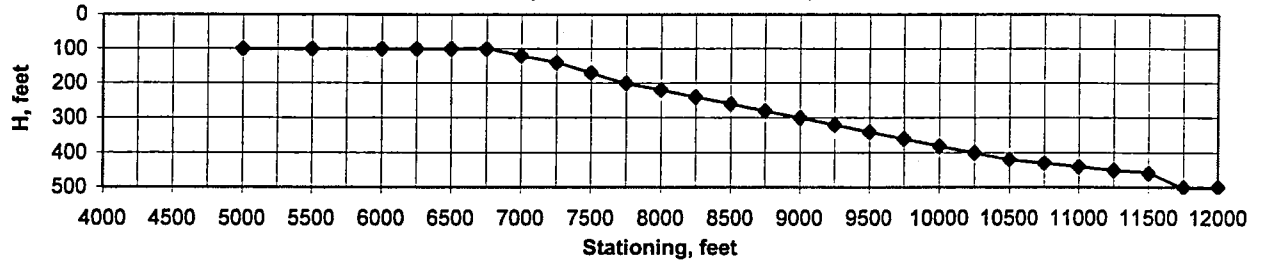


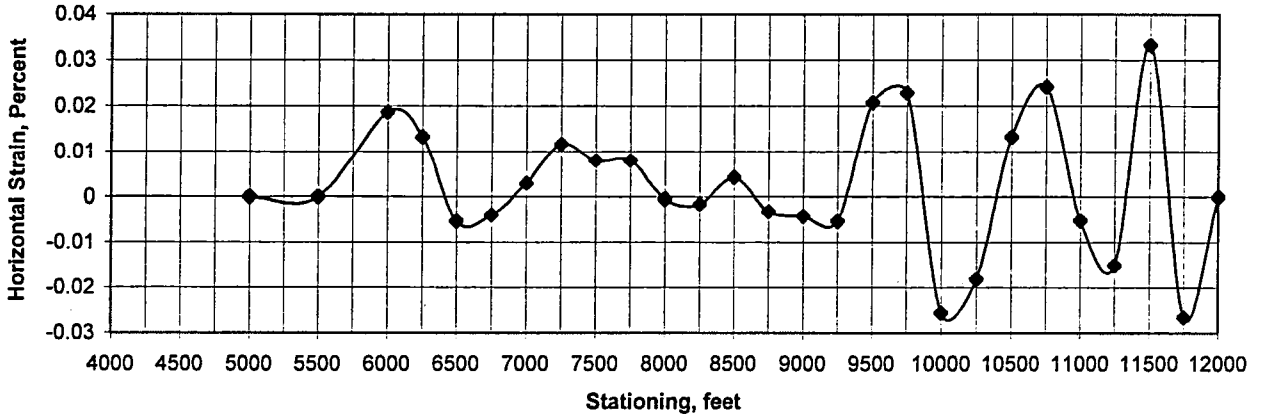
Figure 5

Lee and Shen Analysis - McMicken Dam

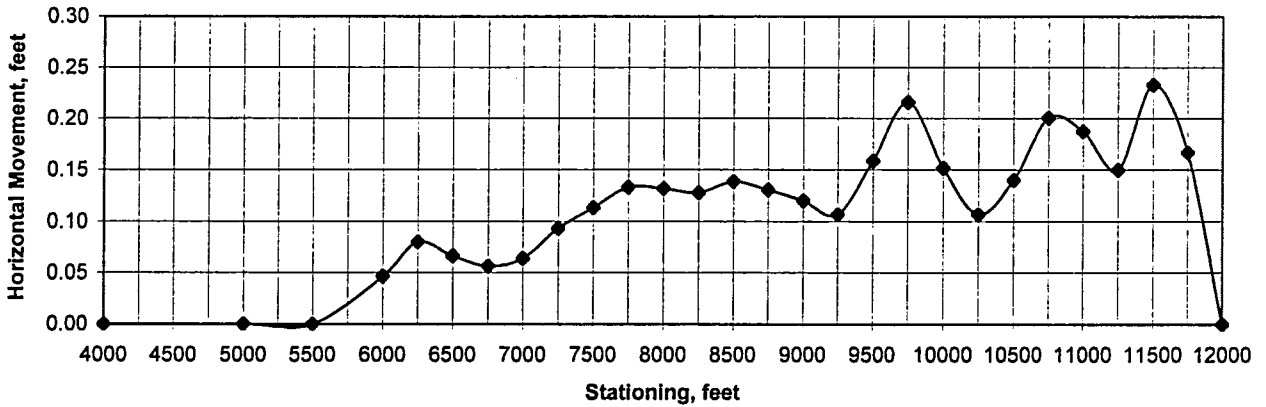
Section B-B' (1955-1982; SHB, 1982) CASE Y-2



Section B-B' (1955-1982; SHB, 1982) CASE Y-2



Section B-B' (1955-1982; SHB, 1982) CASE Y-2



Section B-B' (1955-1982; SHB, 1982) CASE Y-2

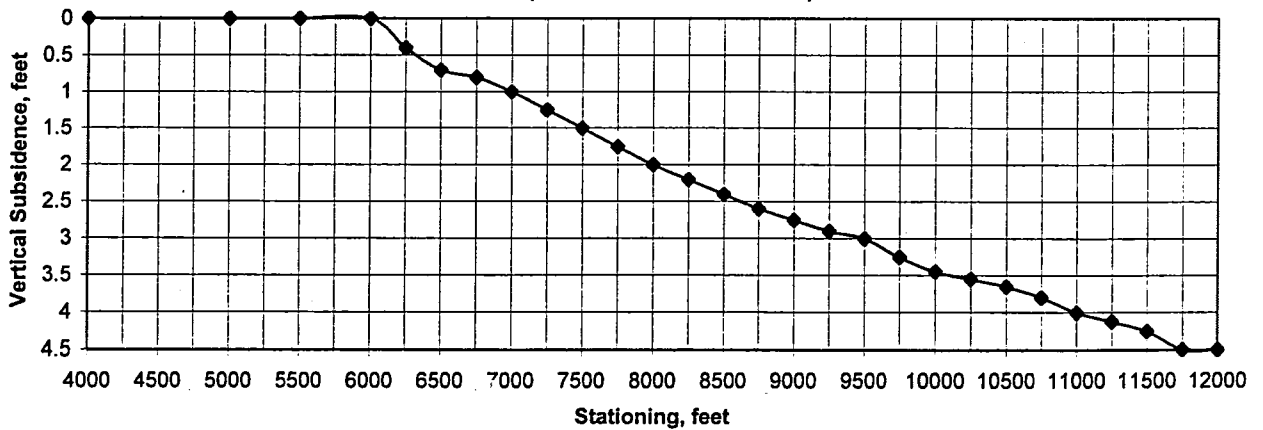


Figure 6 - Well Histories & Modeled Water Levels over Time

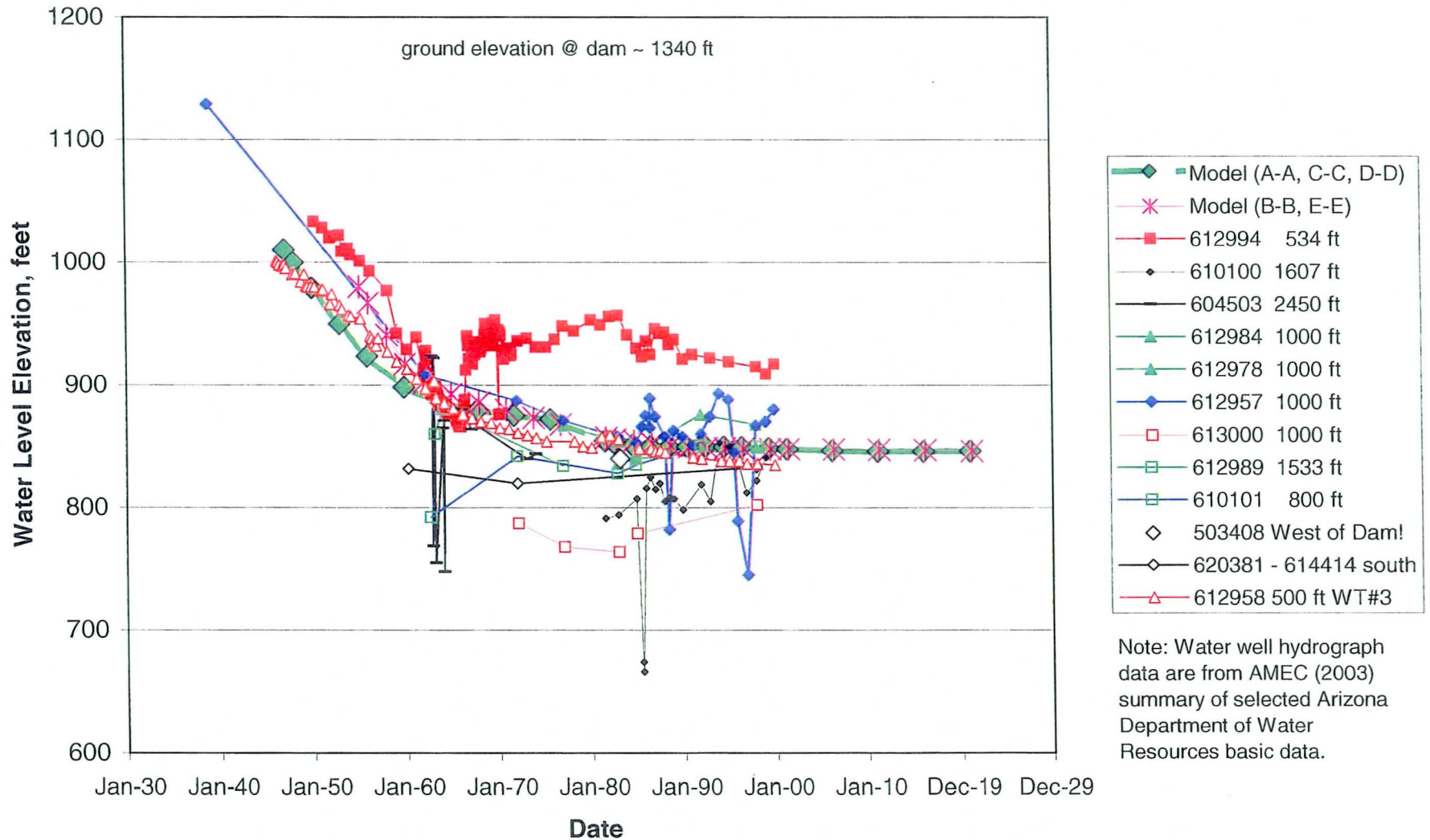
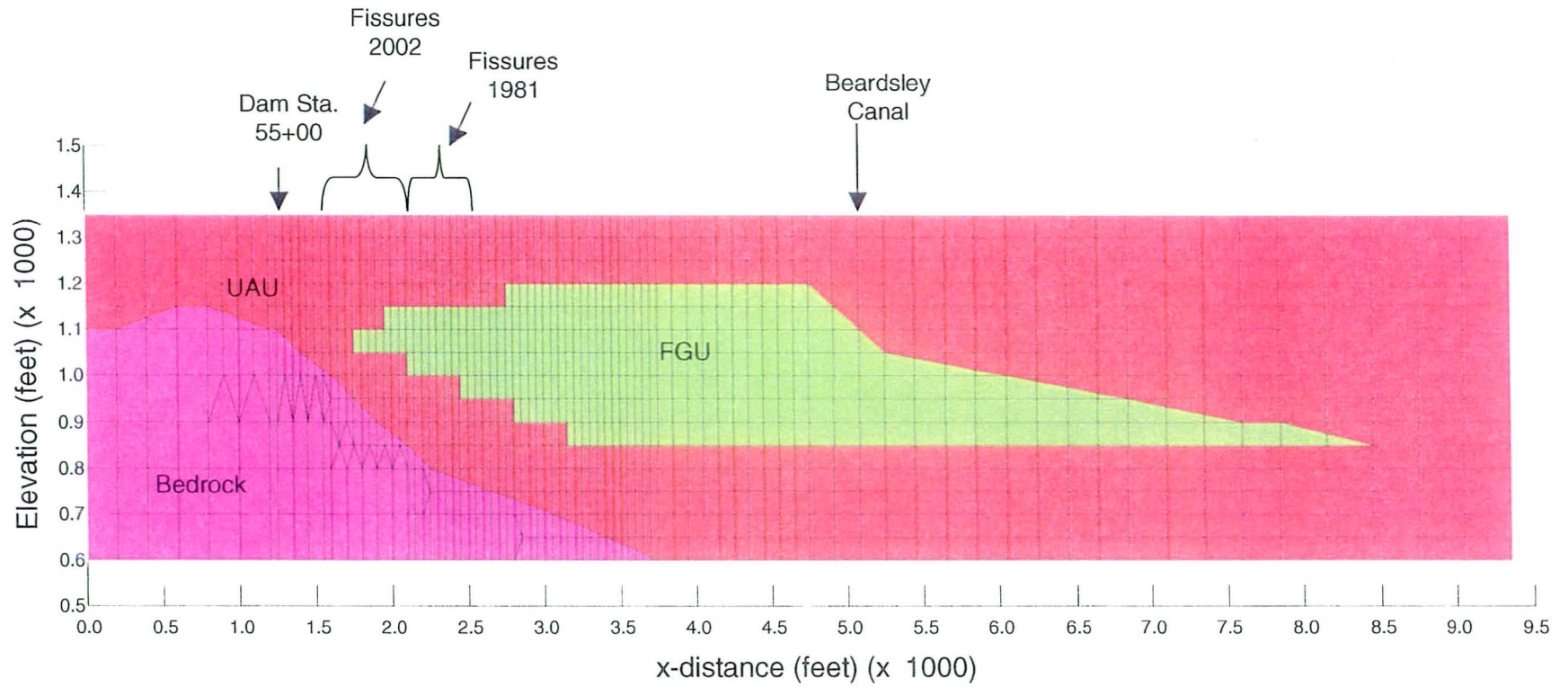


Figure 7
Profile Section A-A'



**Figure 8 - Section A-A' Calibration (1947-1981; NGS)
(modulus variable over time)**

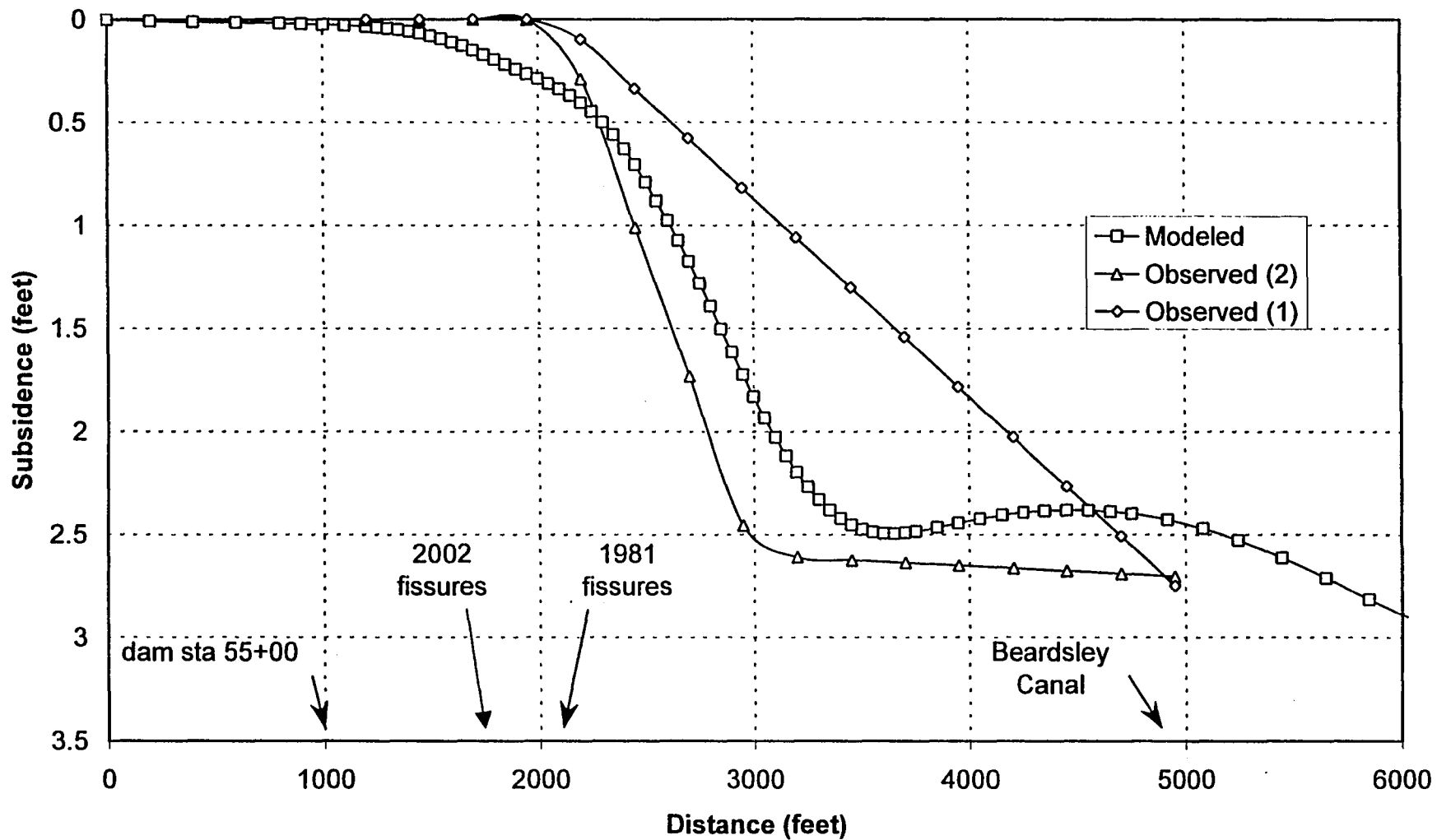
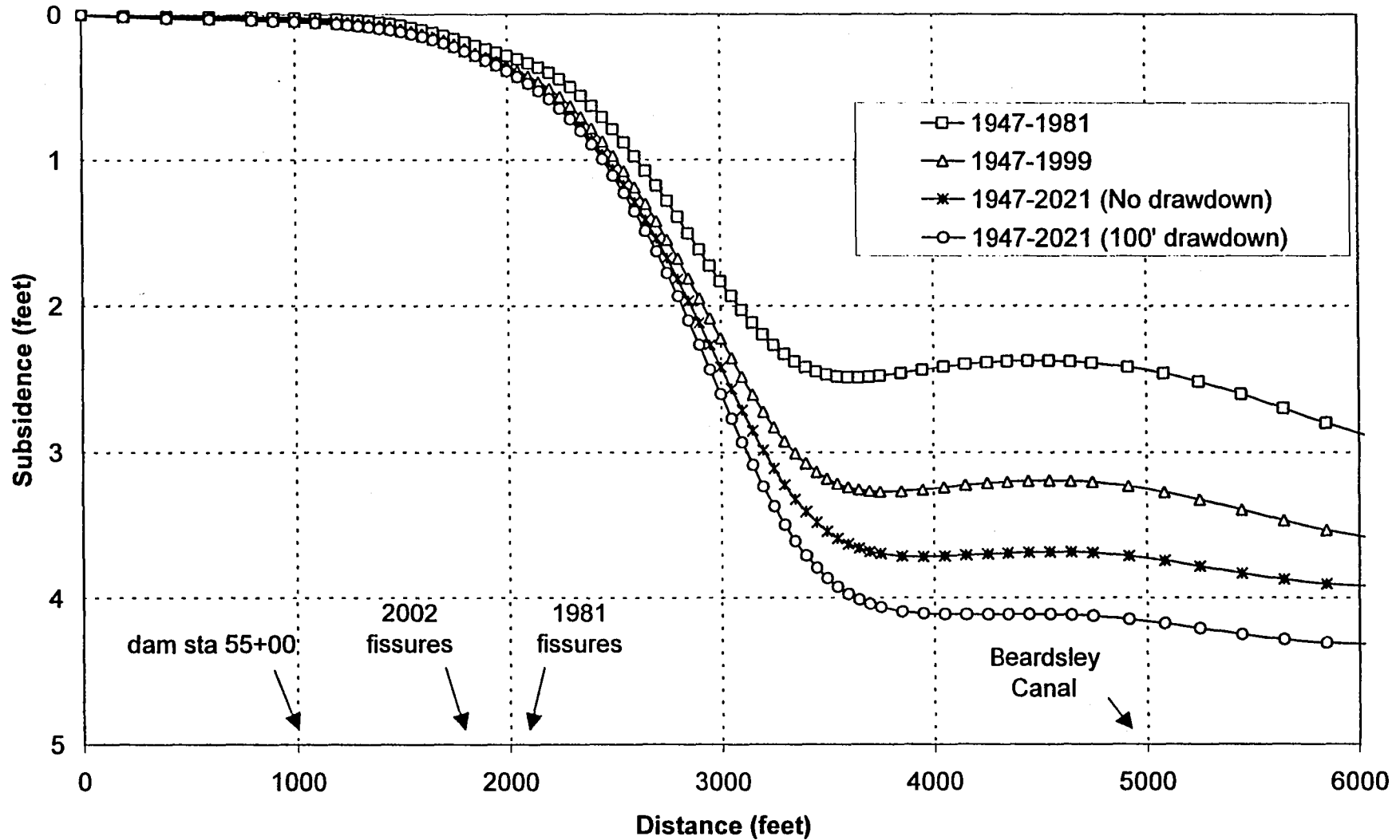


Figure 9 - Section A-A' (variable modulus) Modeled Subsidence



**Figure 10 - Section A-A' (variable modulus)
Modeled vs. INSAR Subsidence**

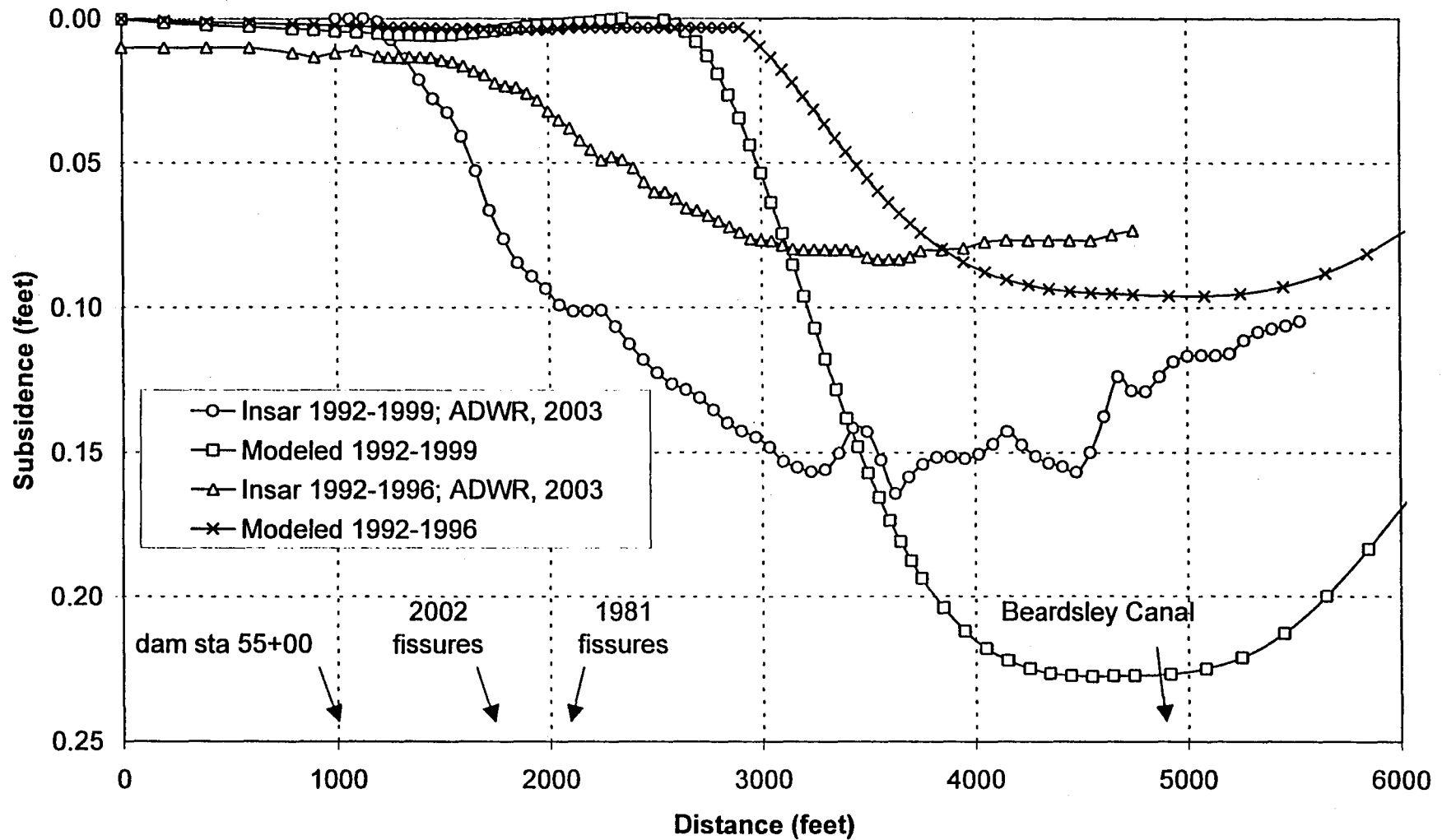
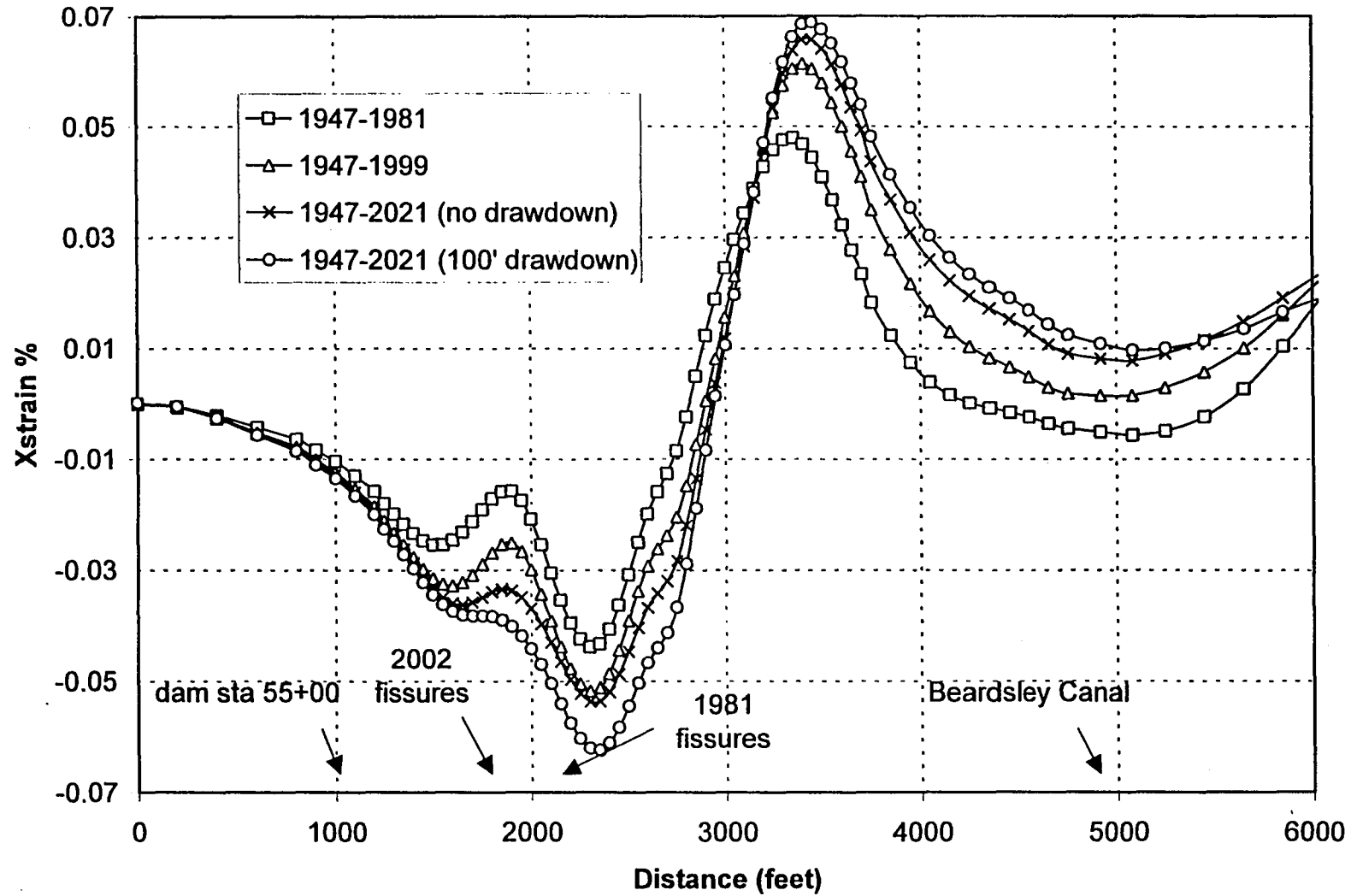


Figure 11 - Section A-A' (variable modulus) Modeled Horizontal Strain



**Figure 12 - Section A-A' Calibration (1947-1981; NGS)
(modulus constant over time)**

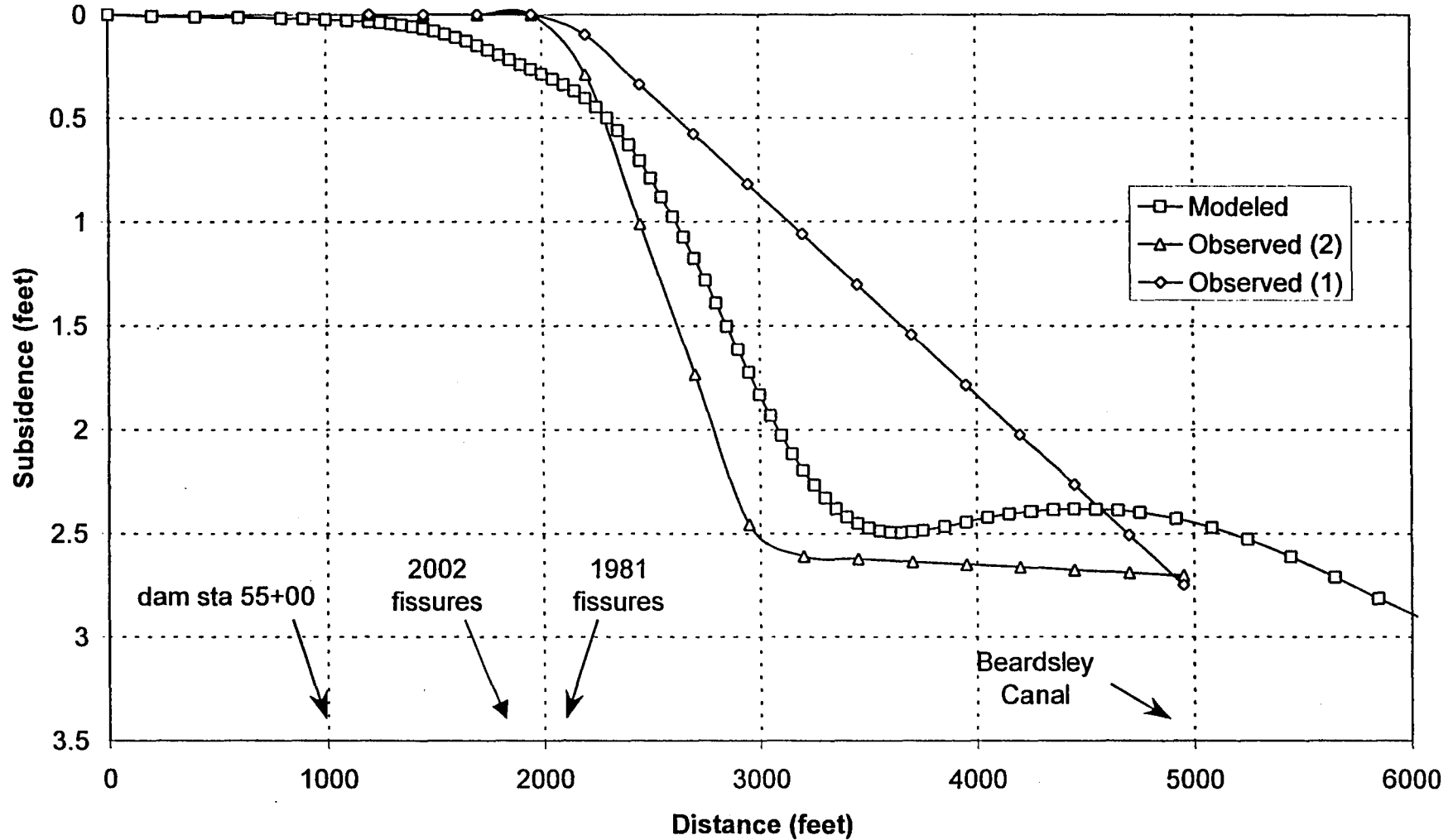
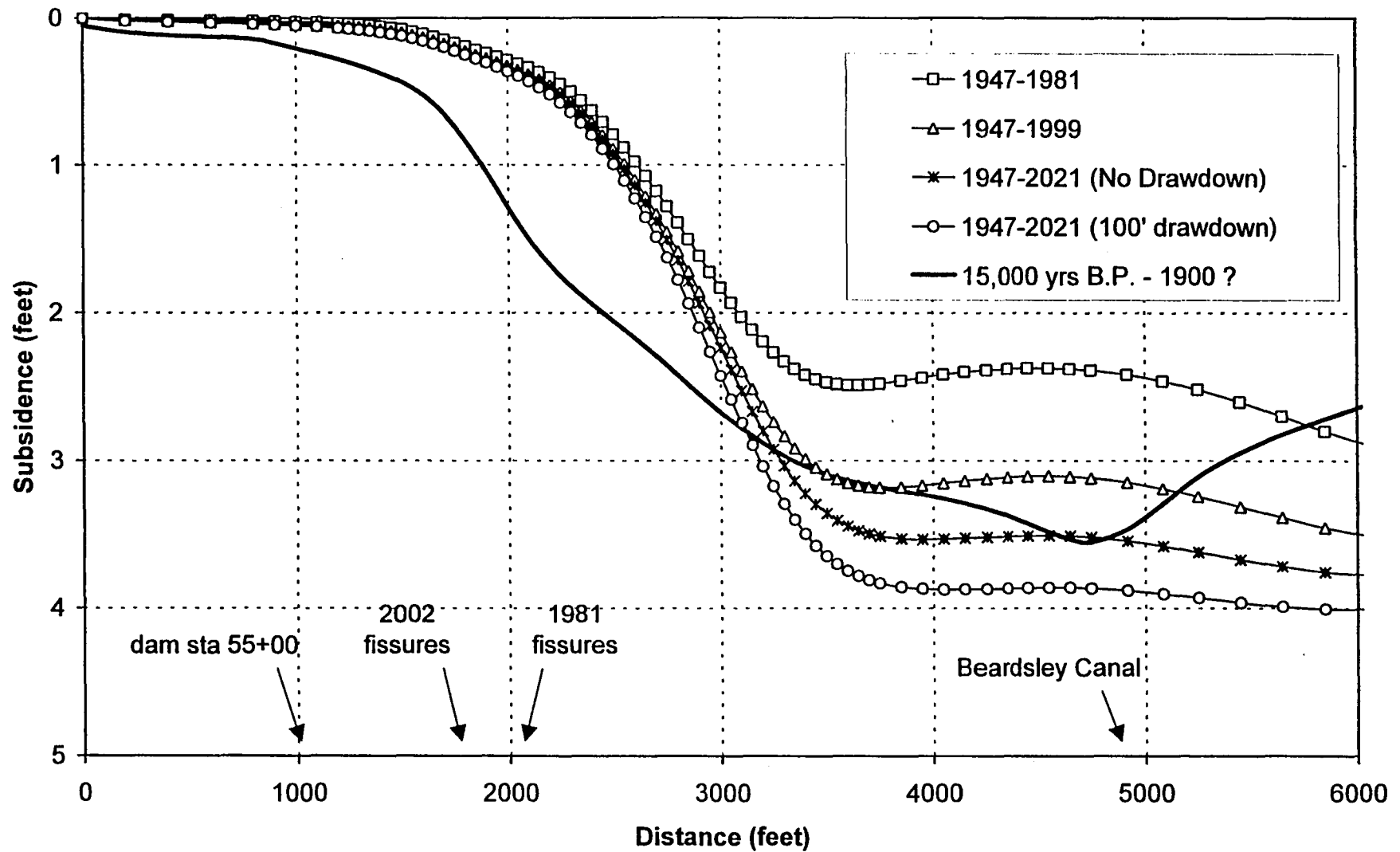


Figure 13 - Section A-A' (modulus constant) Modeled Subsidence



**Figure 14 - Section A-A' (modulus constant)
Modeled vs. INSAR Subsidence**

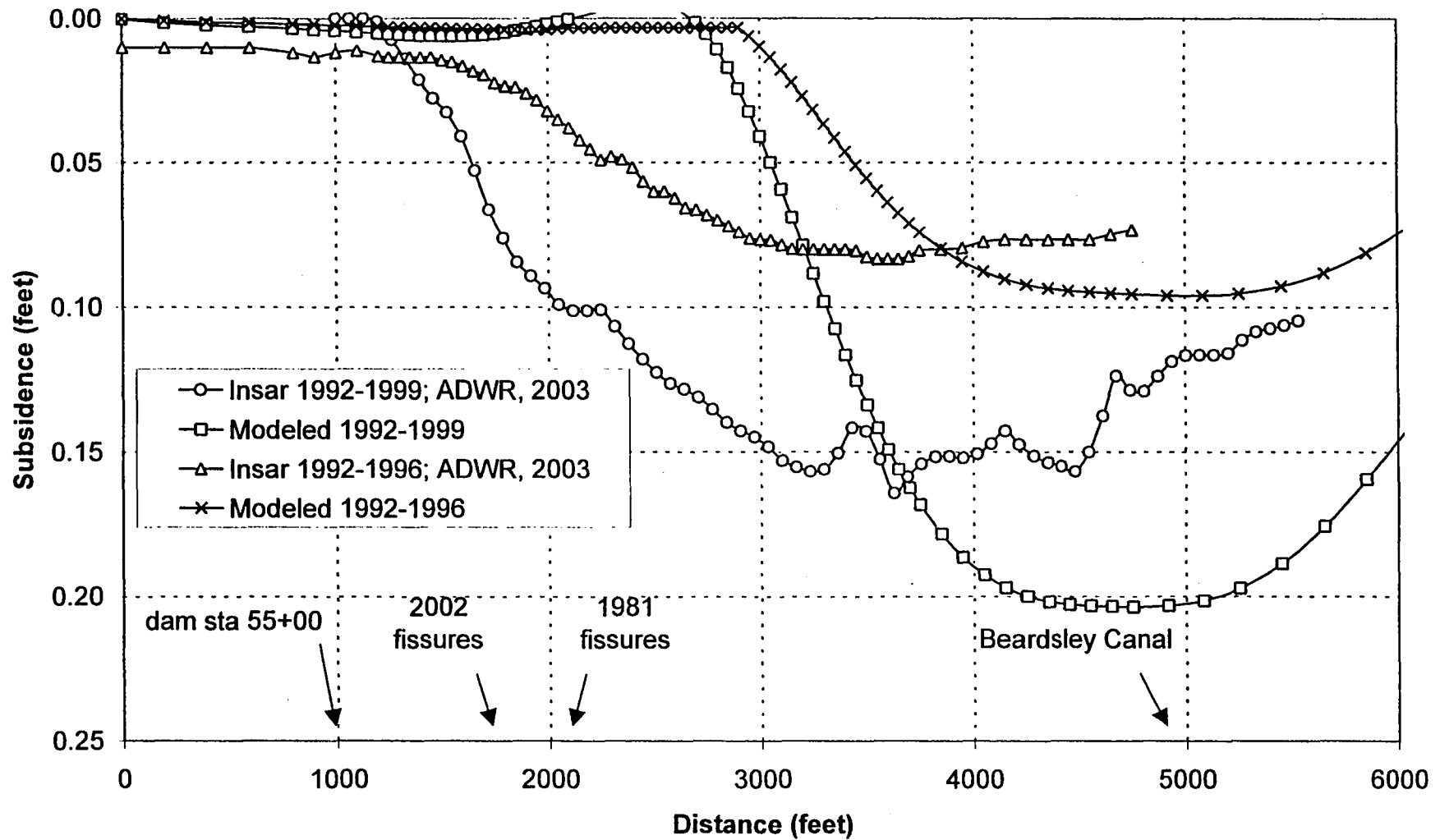


Figure 15 - Section A-A' (modulus constant) Modeled Horizontal Strain

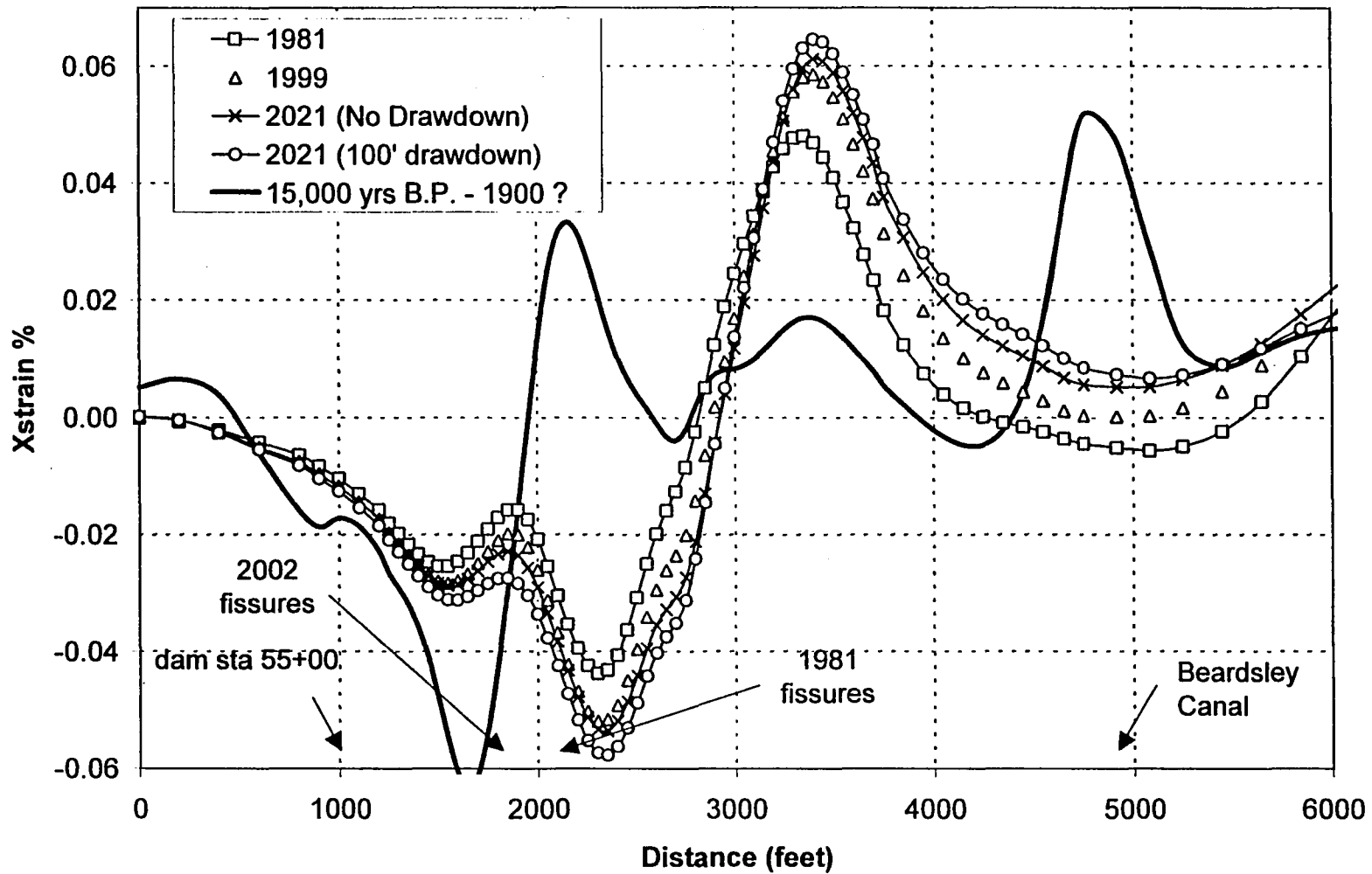
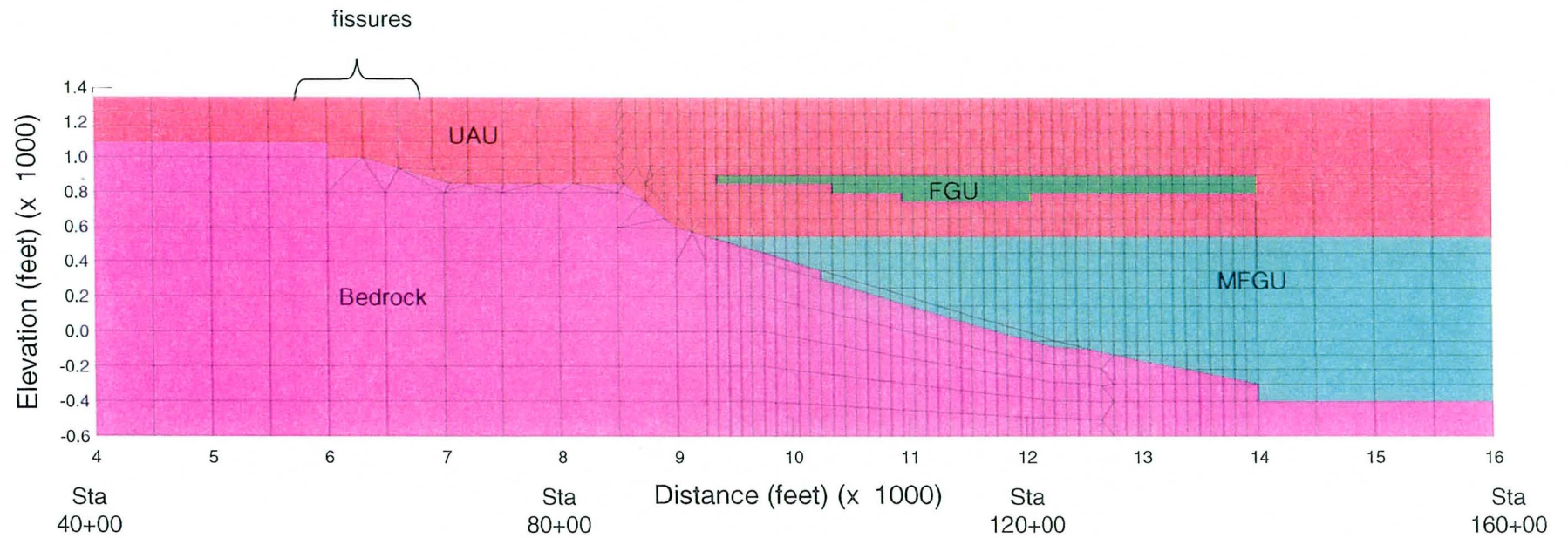


Figure 16

Profile Section B-B Original Geometry (Geometry-1)



**Figure 17 - Section B-B' Initial Calibration Attempt
(before gravity re-interpretation)**

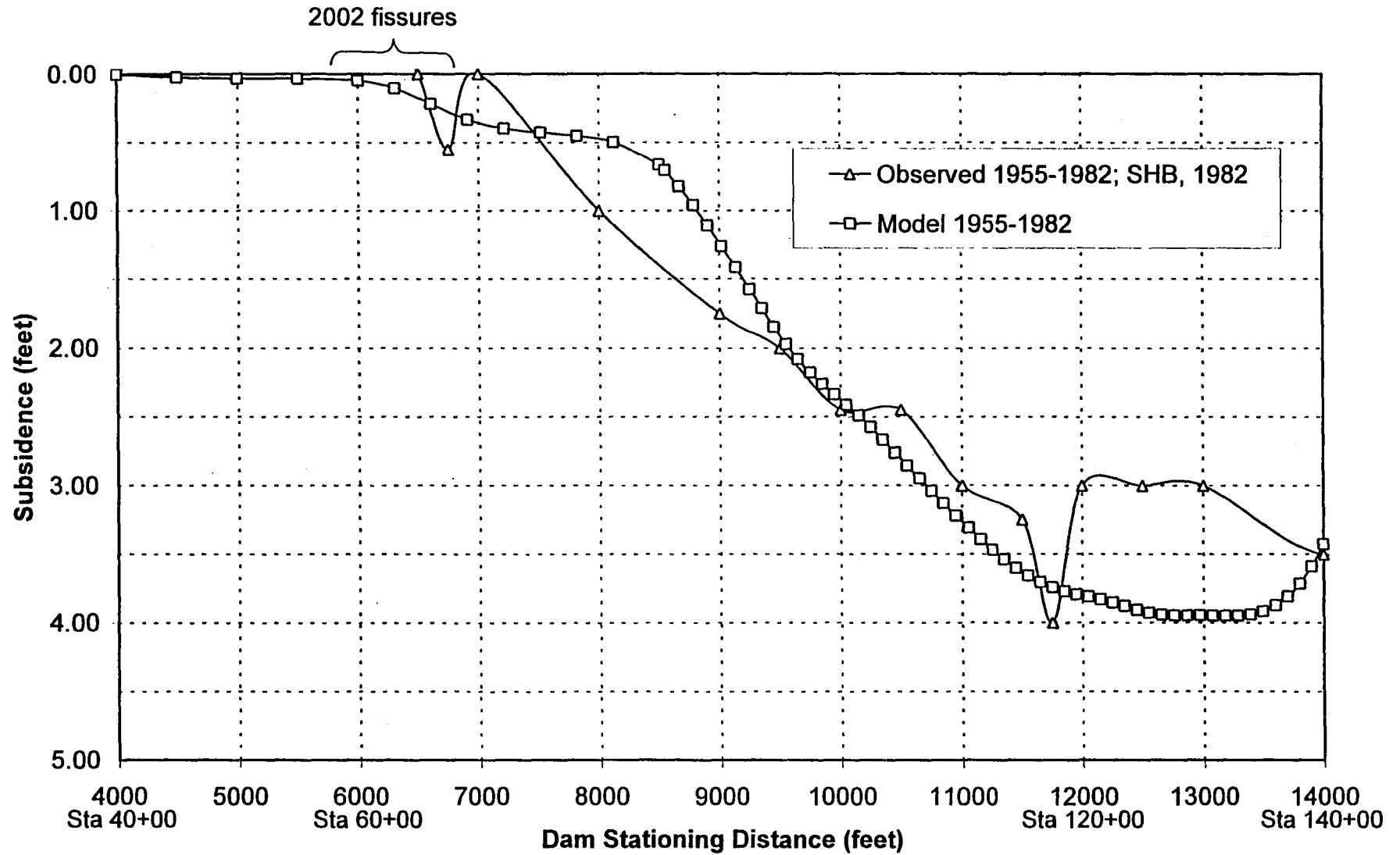


Figure 18

Profile Section B-B' Revised Geometry (Geometry-4)

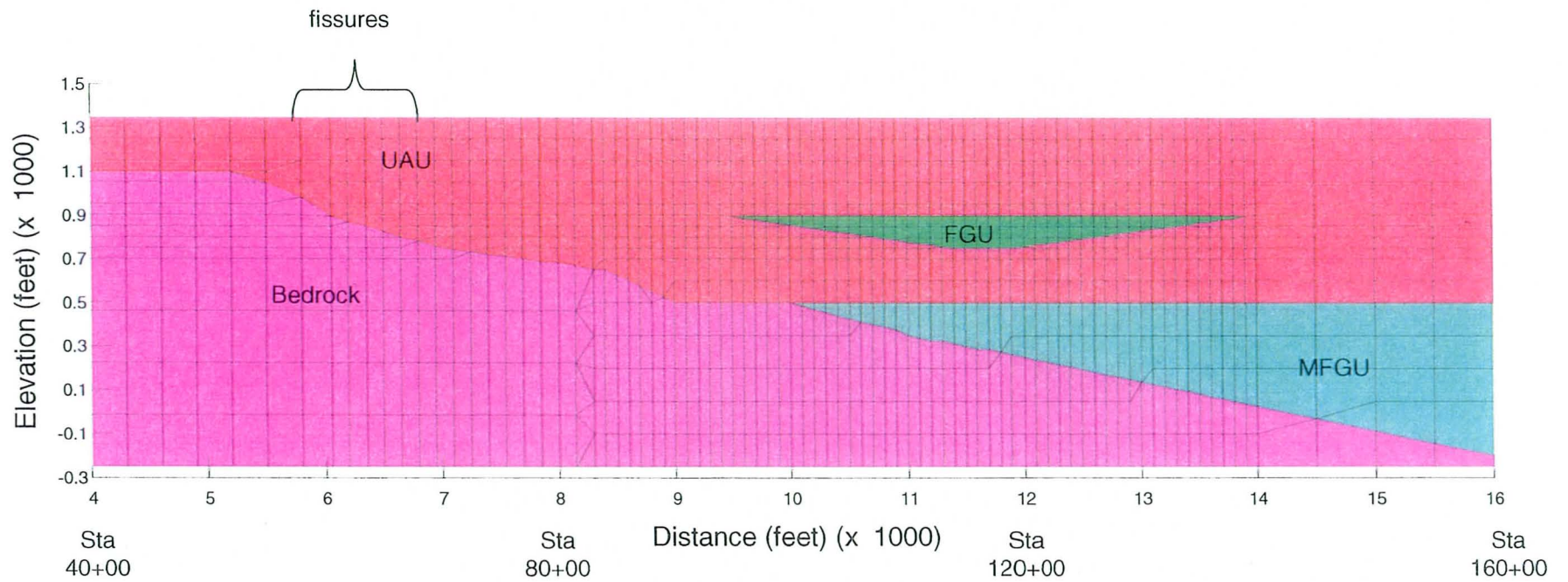


Figure 19 - Section B-B' Calibration (1955-1982; SHB, 1982) after Gravity Re-interpretation of Bedrock Contact

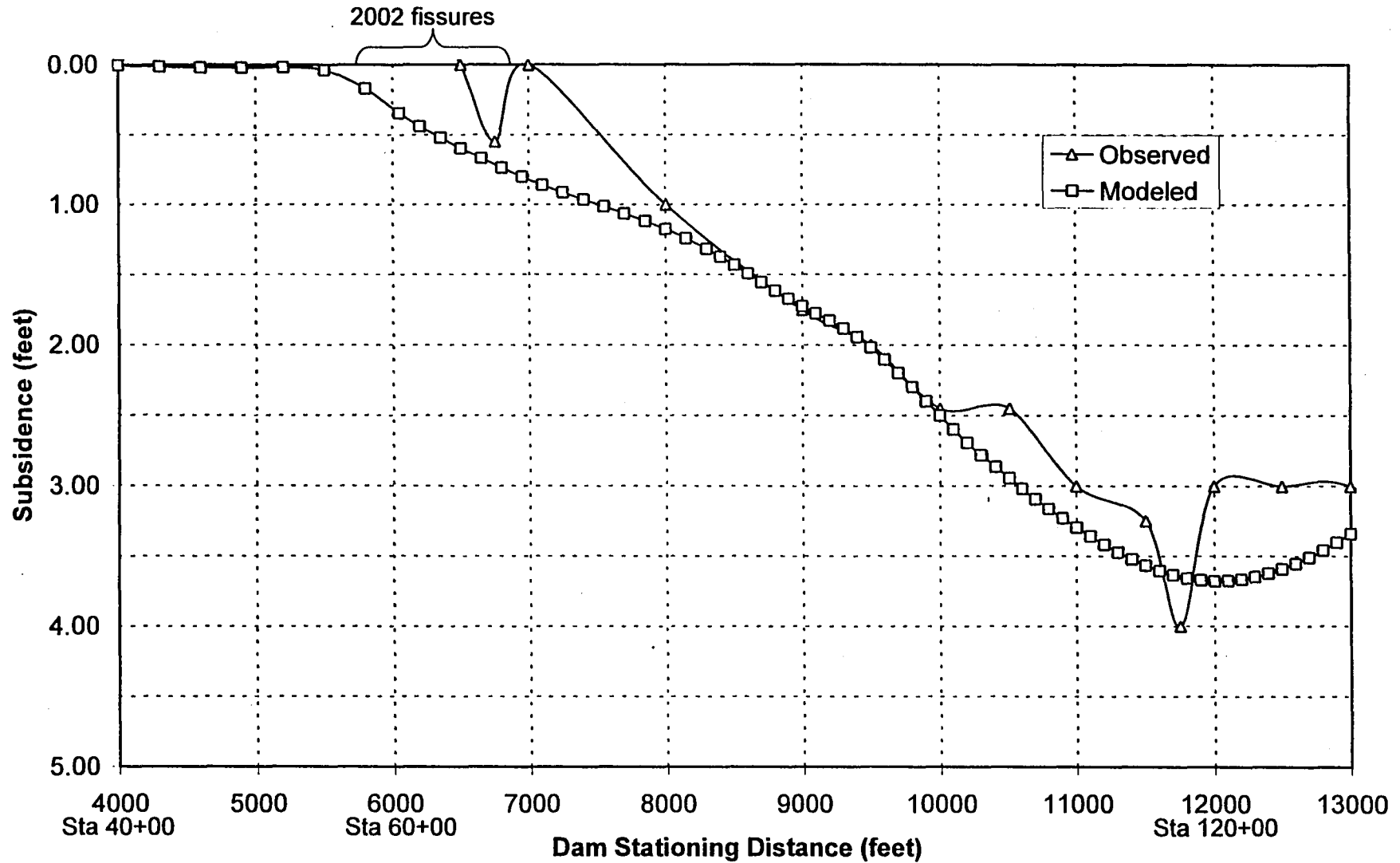


Figure 20 - Section B-B' Modeled vs. Observed Subsidence

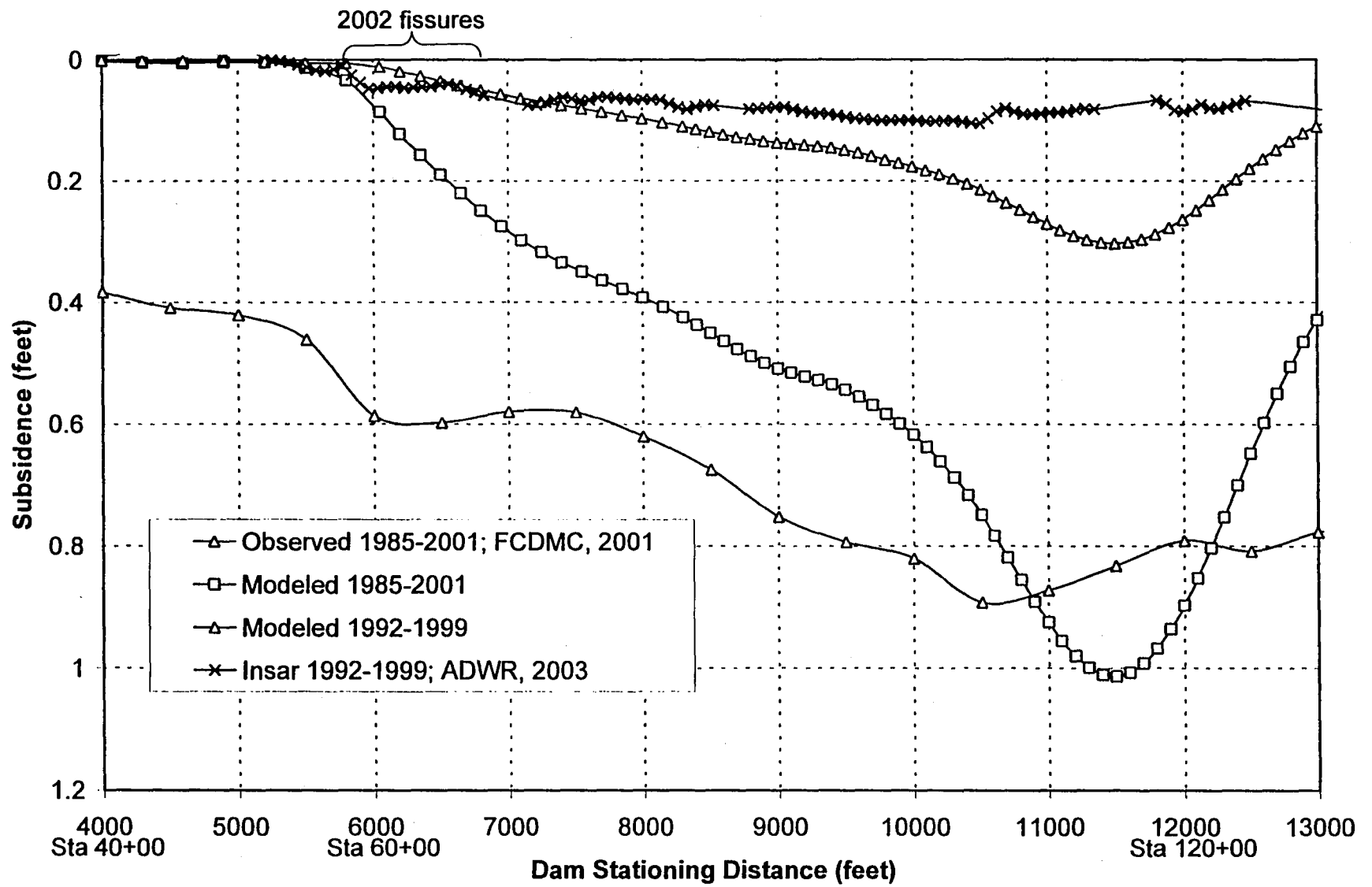


Figure 21 - Section B-B' Modeled Subsidence

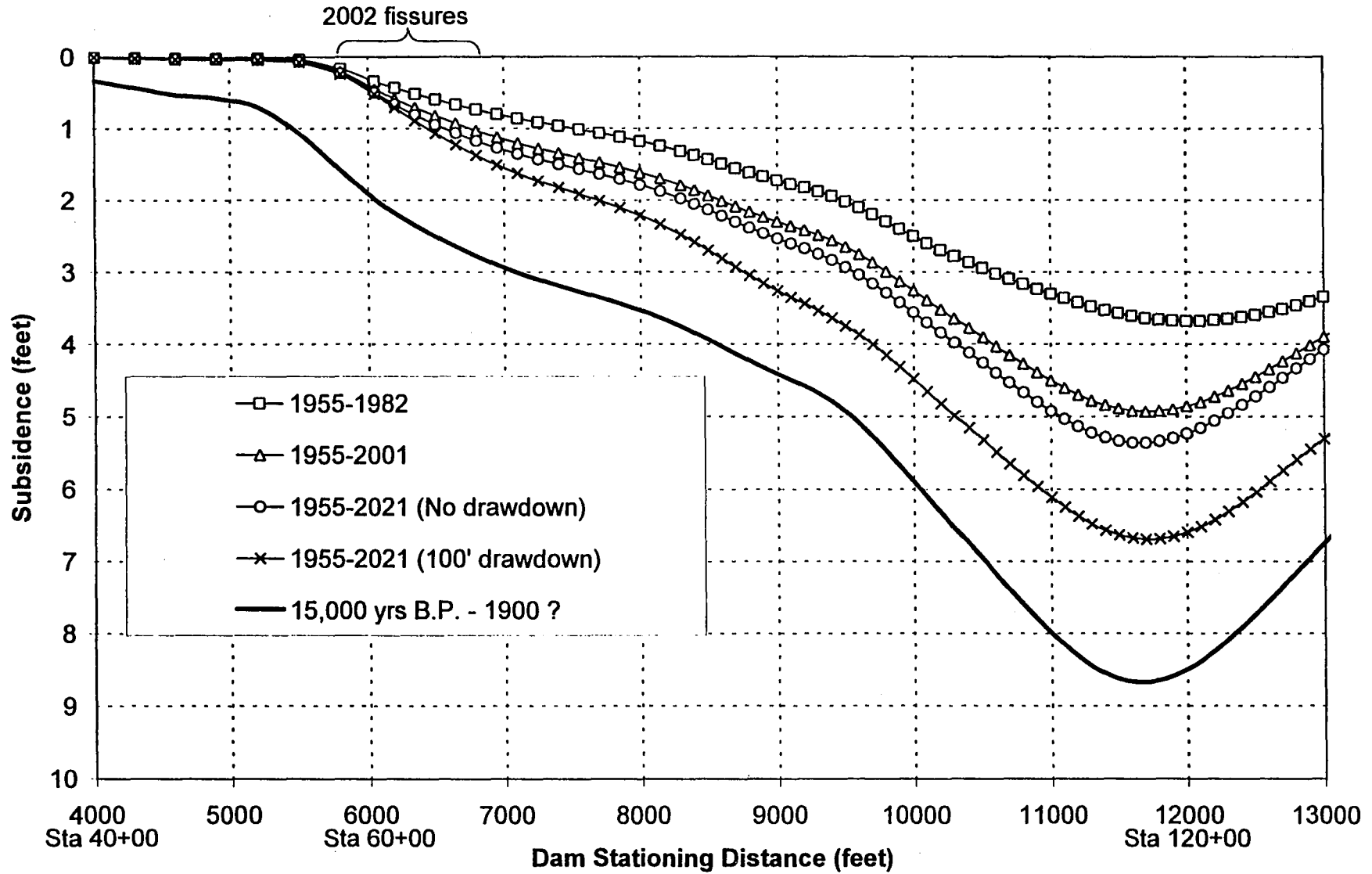


Figure 22 - Section B-B' Modeled Horizontal Strain

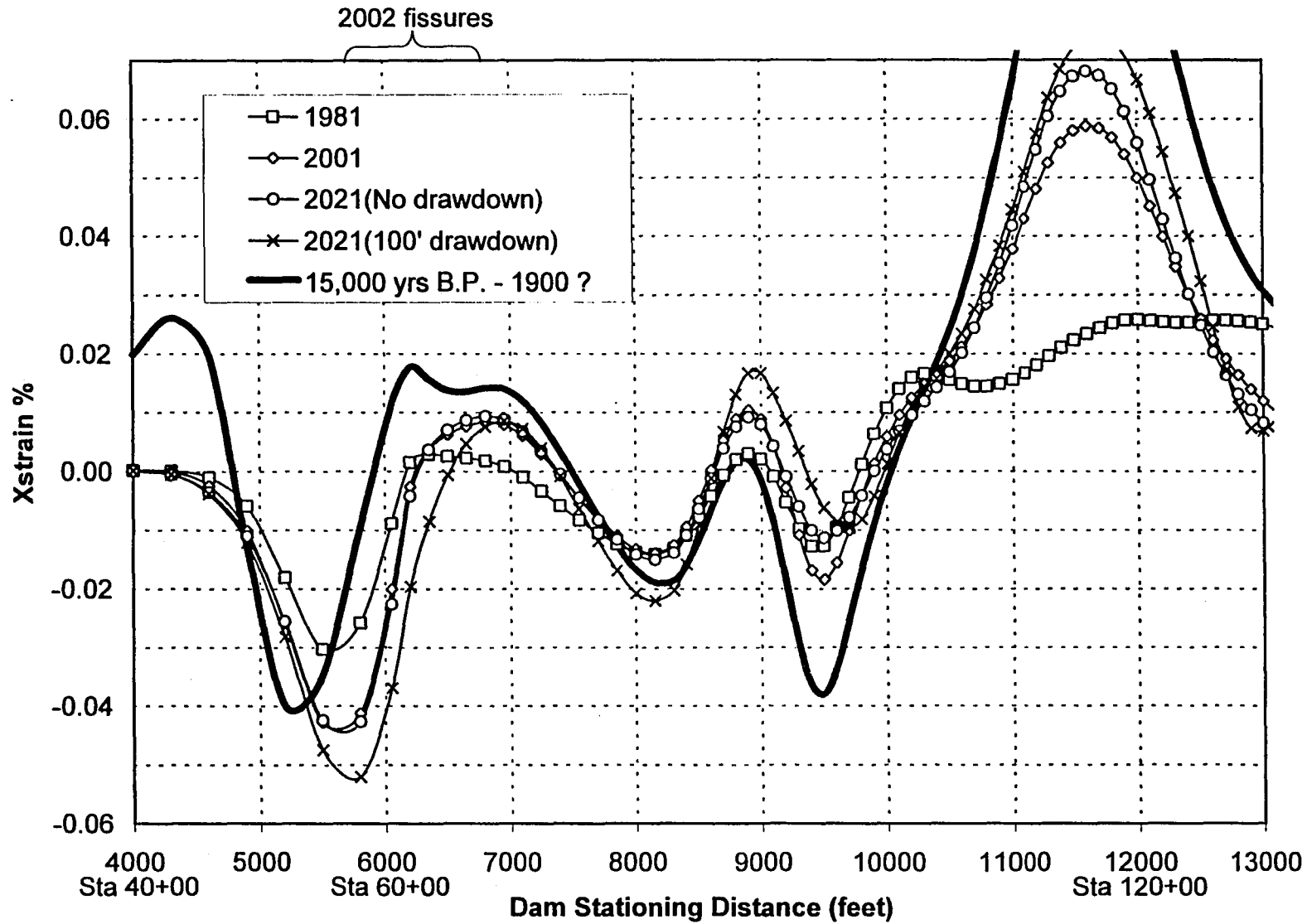


FIGURE 23
Profile Section C-C'

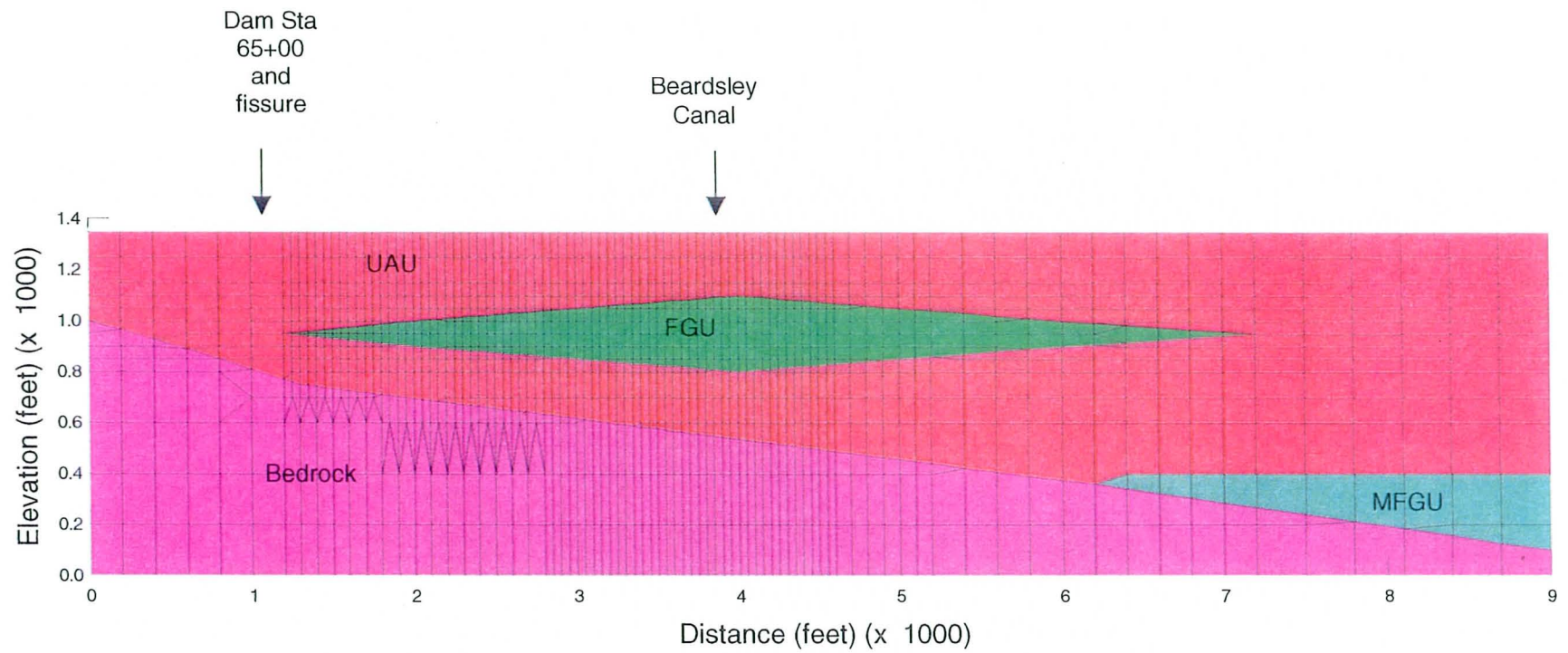


Figure 24 - Section C-C' & D-D' Subsidence Calibration (1947-1981; NGS)

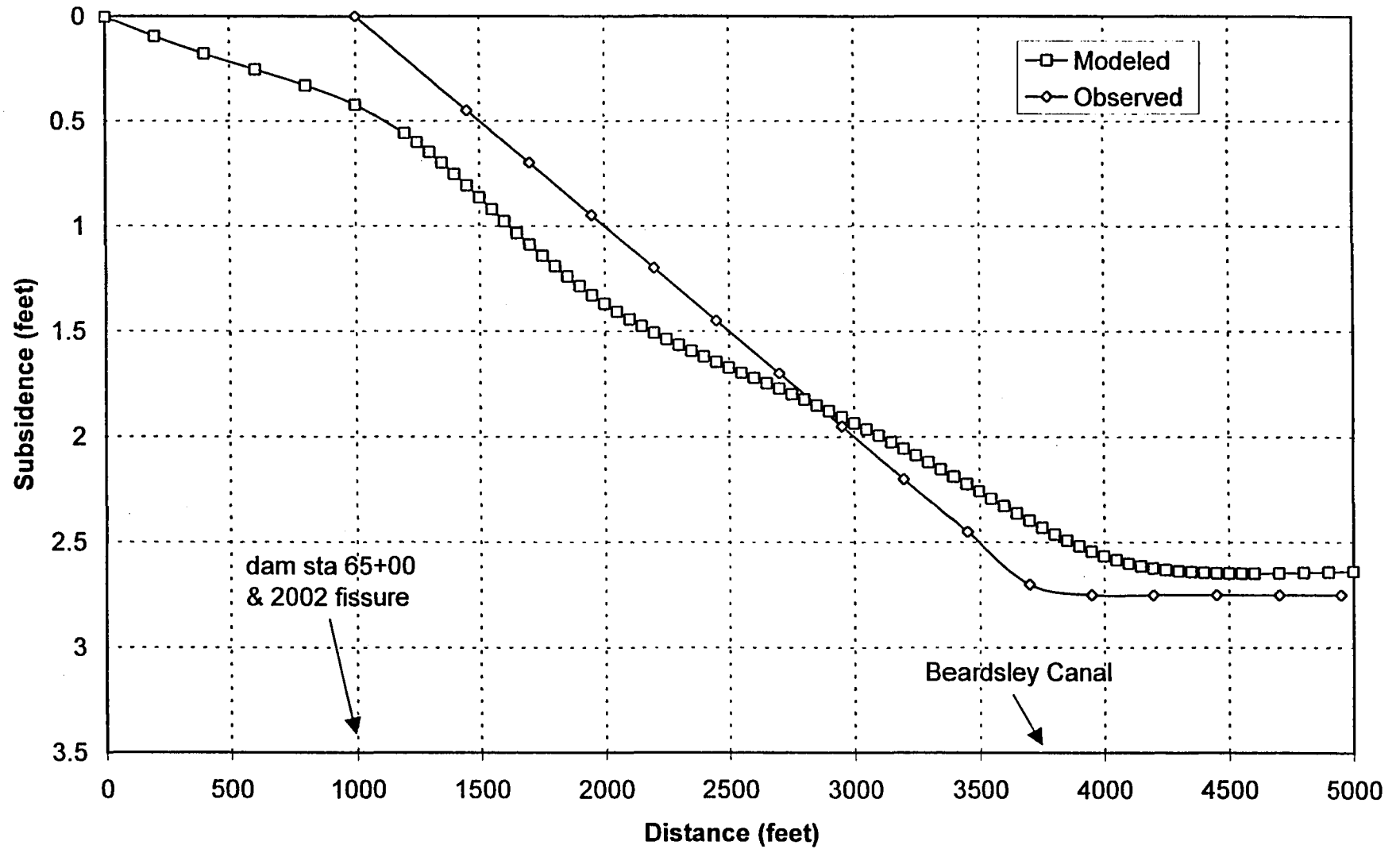


Figure 25 - Section C-C' InSAR vs. Modeled Subsidence

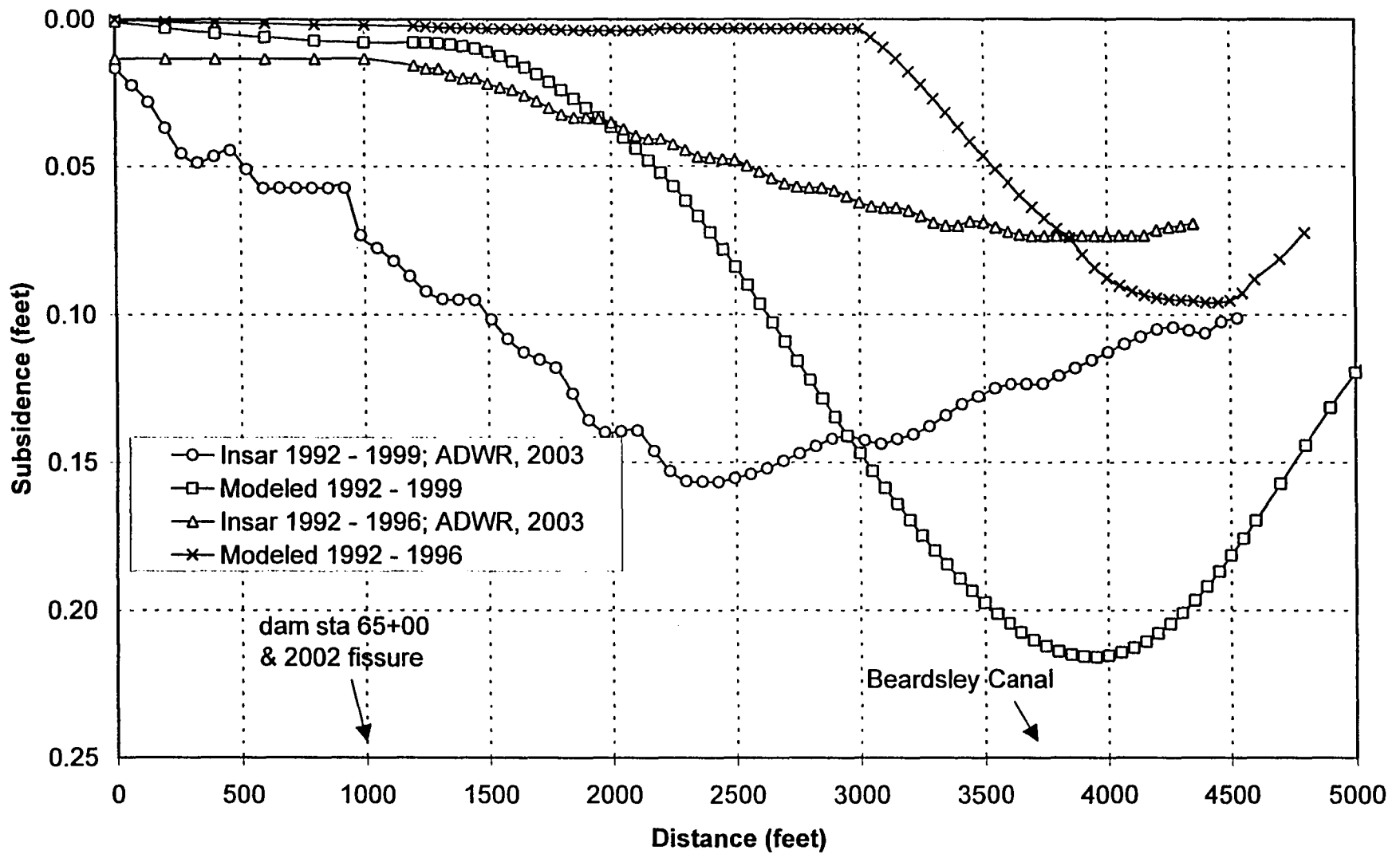


Figure 26 - Section C-C' Modeled Subsidence

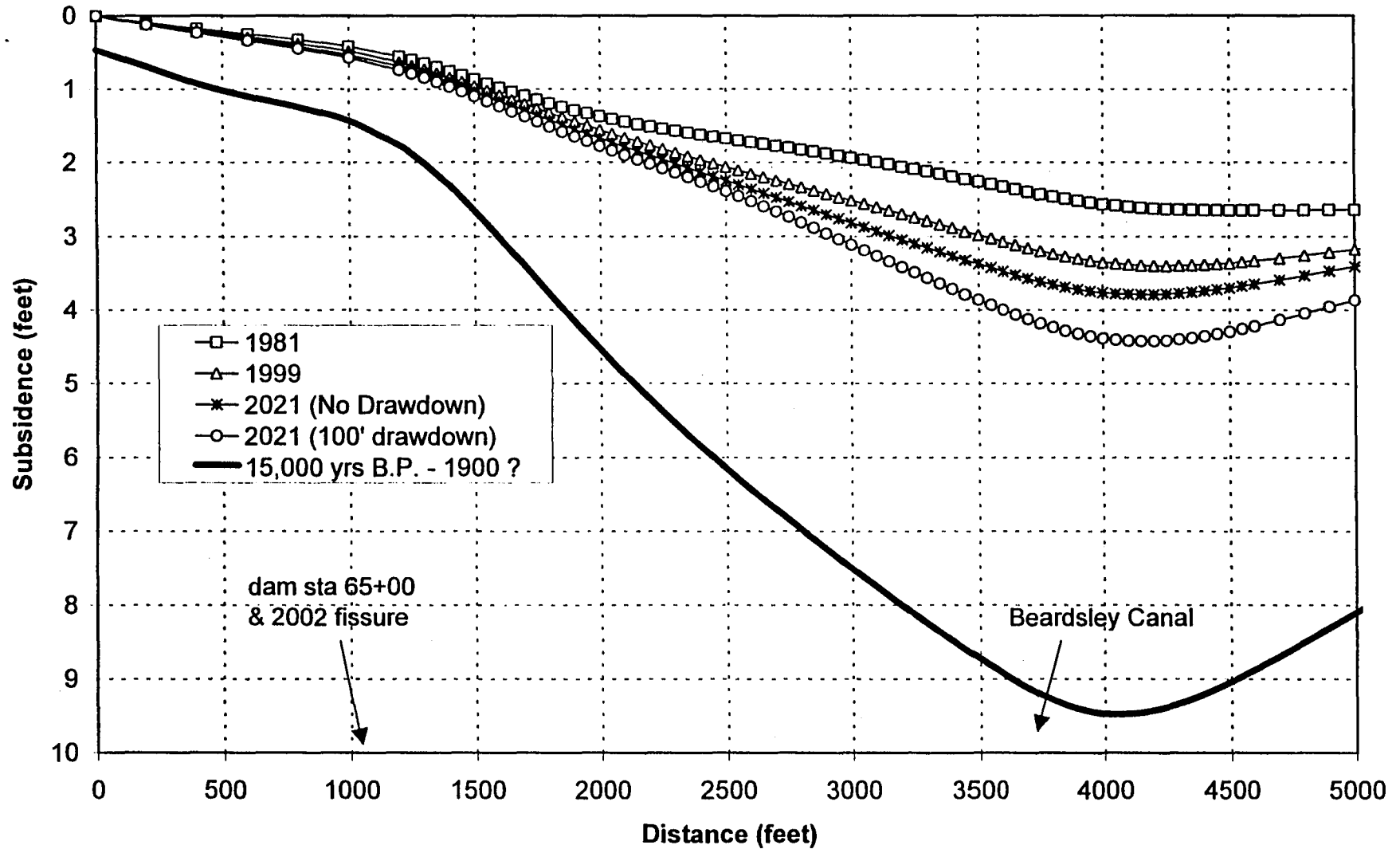


Figure 27 - Section C-C' Modeled Horizontal Strain

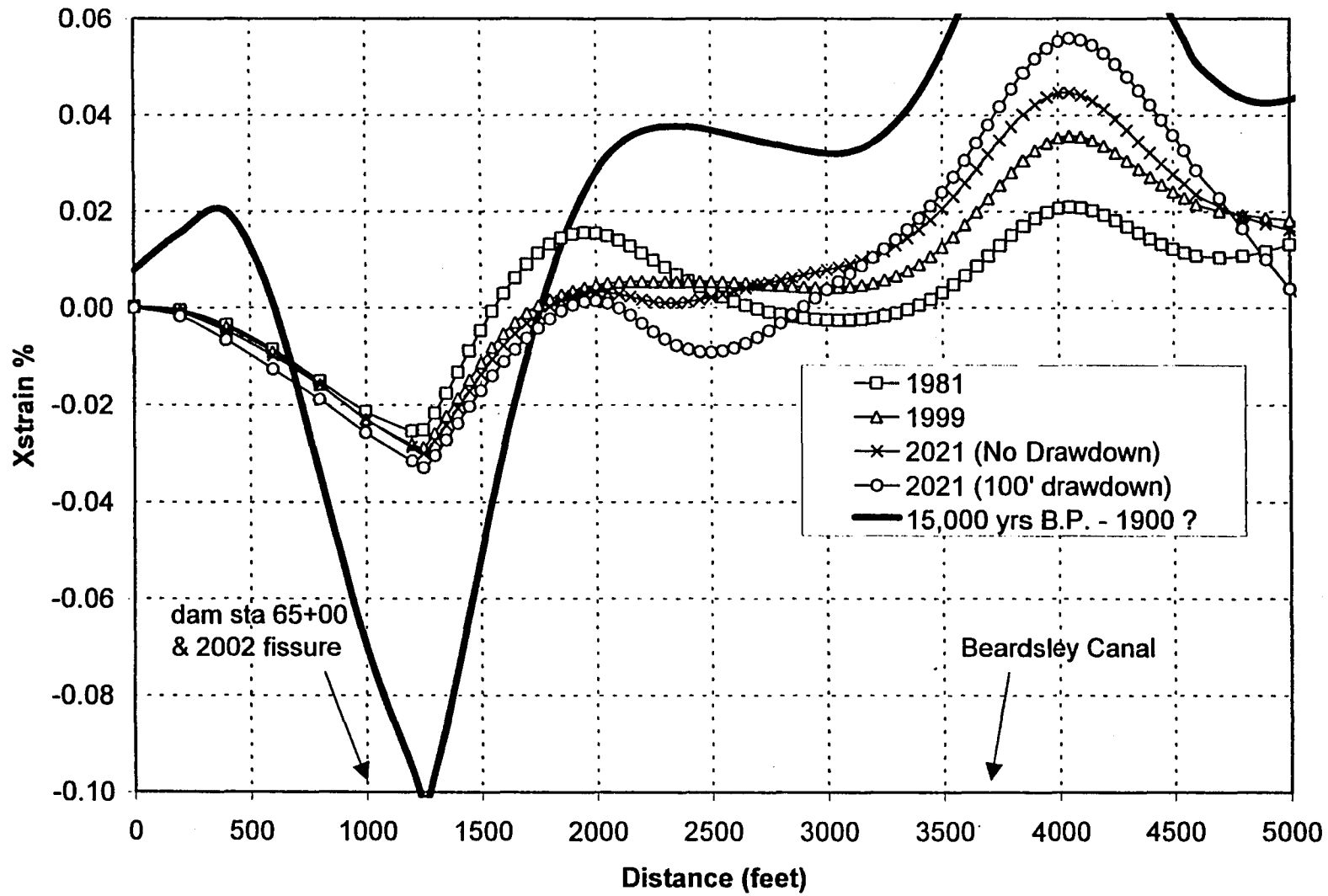


Figure 28
Profile Section D-D'

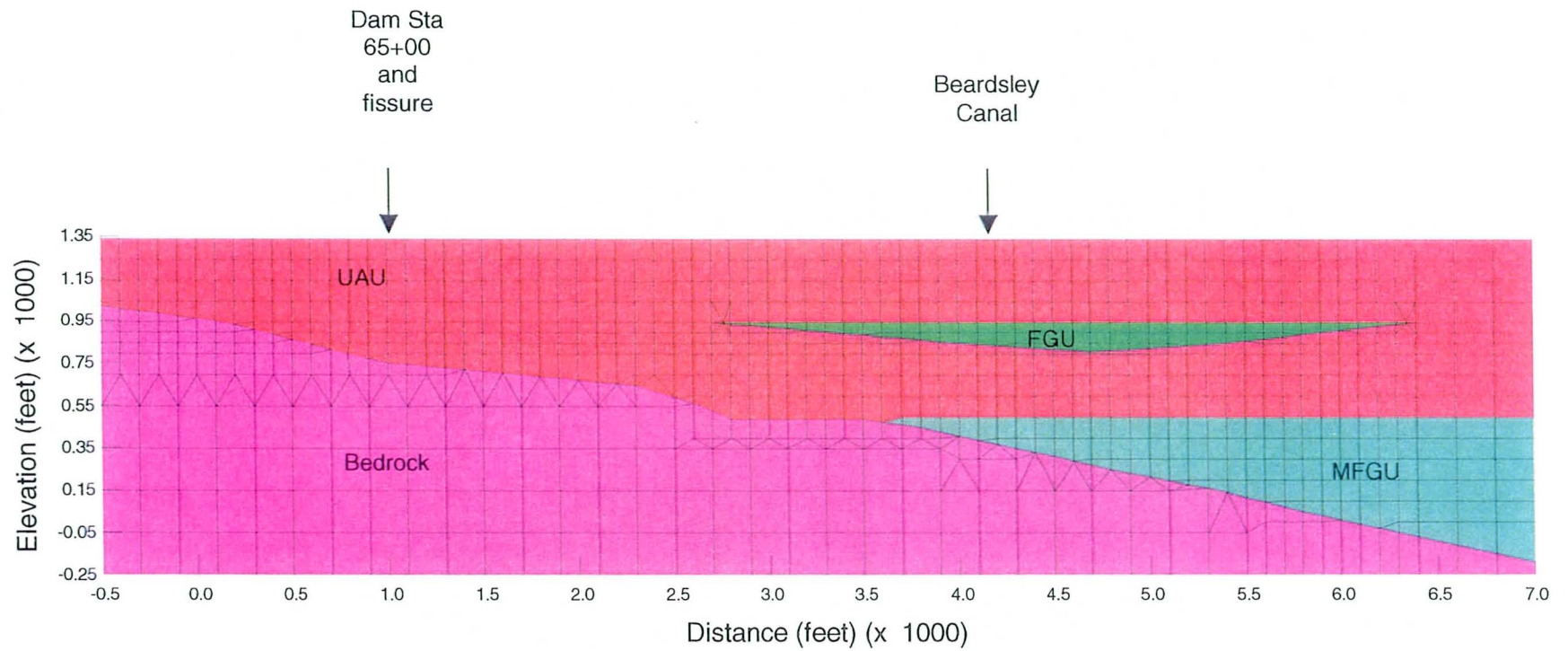


Figure 29 - Section D-D' (1992-1999) Modeled vs. InSAR Subsidence

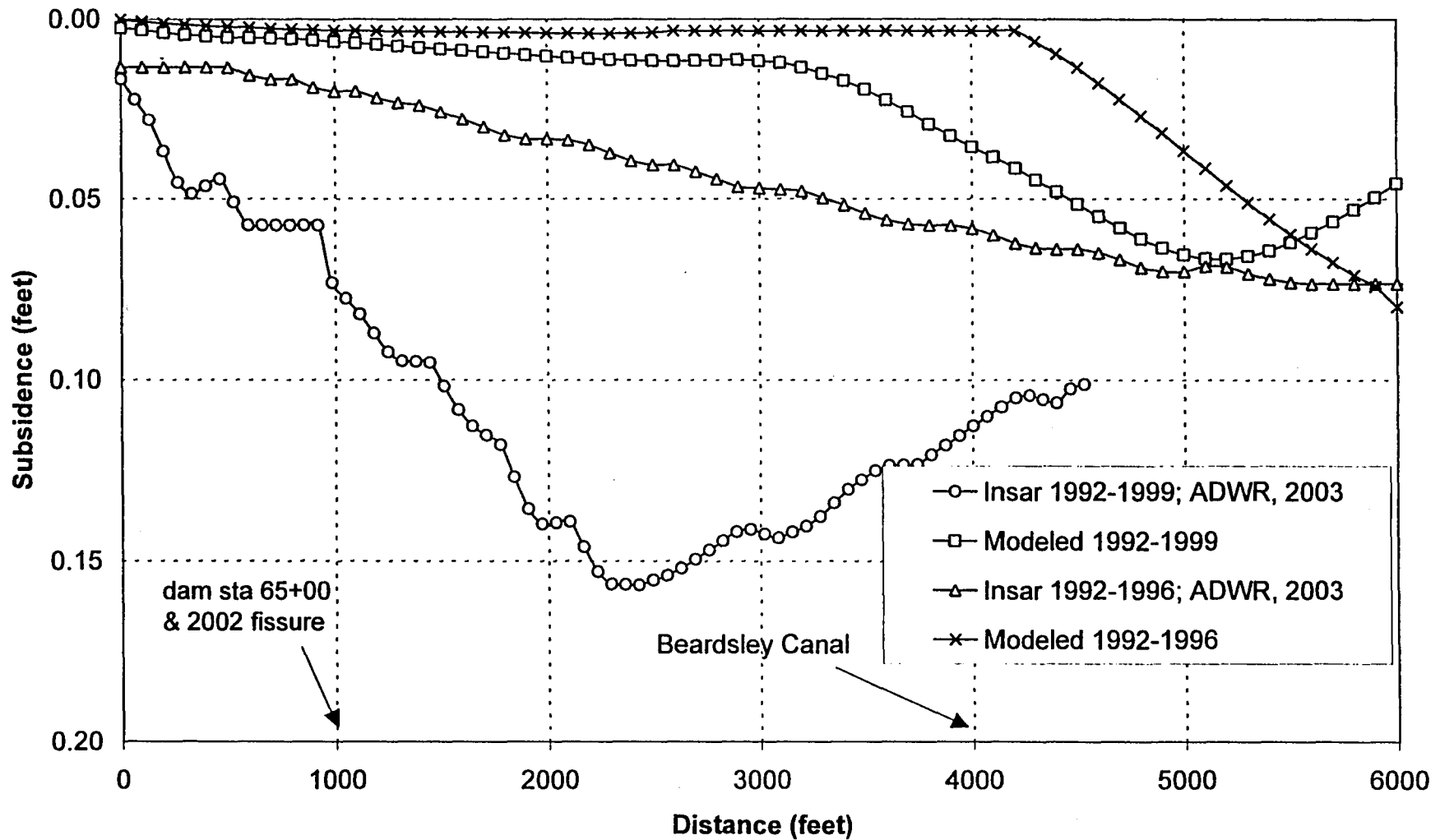


Figure 30 - Section D-D' Modeled Subsidence

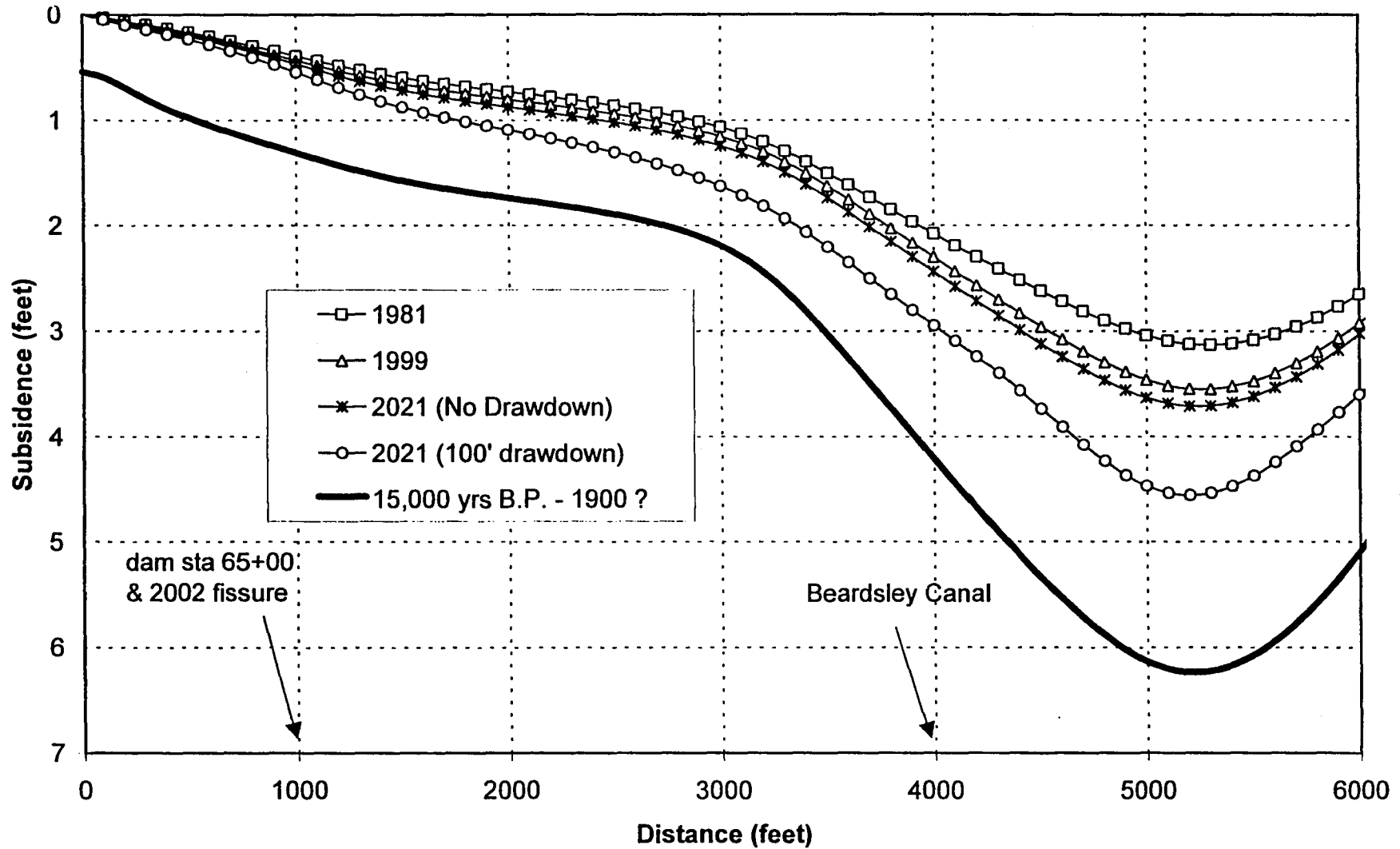


Figure 31 - Section D-D' Modeled Horizontal Strain

